

Drizzle in stratiform boundary layer clouds. Part I: Vertical and horizontal structure

R. WOOD*

The Met Office, Bracknell, Berkshire, UK.

April 1, 2004

Abstract

Detailed observations of stratiform boundary layer clouds on twelve days are examined with specific reference to drizzle formation processes. The clouds differ considerably in mean thickness, liquid water path (*LWP*) and droplet concentration. Cloud base precipitation rates contents differ by a factor of 20 between cases. The lowest precipitation rate is found in the case with the highest droplet concentration even though this case had by far the highest *LWP*, suggesting that drizzle can be severely repressed in polluted clouds.

The vertical and horizontal structure of cloud and drizzle liquid water and bulk microphysical parameters are examined in detail. The adiabaticity of the cloud liquid water content is found to decrease with increasing precipitation rate. In general, the highest concentration of $r > 20\mu\text{m}$ drizzle drops is found towards the top of the cloud and the mean volume radius of the drizzle drops increases monotonically from cloud top to base. The resulting precipitation rates are largest at the cloud base but decrease markedly only in the upper third of the cloud. Below cloud, precipitation rates decrease markedly with distance below base due to evaporation, and are broadly consistent in most cases with the results from a simple sedimentation-evaporation model. Evidence is presented that suggests evaporating drizzle is cooling regions of the subcloud layer which could result in dynamical feedbacks. A composite power spectrum of the horizontal spatial series of precipitation rate is found to exhibit a power-law scaling from the smallest scales to close to the maximum observable scale (~ 30 km). The exponent is considerably lower (1.1-1.2) than corresponding exponents for *LWP* variability obtained in other studies (~ 1.5 -2) demonstrating that there is relatively more variability of drizzle on small scales. Singular measures analysis shows that drizzle fields are much more intermittent than the cloud liquid water content fields, consistent with a drizzle production process that depends strongly upon liquid water content. The adiabaticity of the clouds, which can be modeled as a simple balance between drizzle loss and turbulent replenishment is found to decrease as the timescale for drizzle loss becomes significantly shorter than the eddy turnover timescale. Finally, the precipitation rates do not compare particularly well with scalings derived from recent observations of subtropical stratocumulus clouds, which may reflect the more diverse range of forcing conditions in this study.

*Current author address: Atmospheric Sciences, Box 351640, University of Washington, Seattle, WA, 98102, USA. BRITISH CROWN COPYRIGHT

1. Introduction

Drizzle is an important phenomenon in marine low cloud because (a) even low precipitation rates are comparable energetically to other forcings, and (b) drizzle is common in the marine boundary layer (MBL) (Petty, 1995). Drizzle production is dependent upon the interplay between microphysical, thermodynamic and dynamical processes (Mason, 1952; Nicholls, 1987; Baker, 1993; Austin et al., 1995b; Feingold et al., 1996). The hypothesis (Liou and Ou, 1989; Albrecht, 1989) that in MBL clouds enhanced aerosol concentrations may suppress drizzle and prolong cloud lifetime (the so-called *second indirect effect*, or *aerosol-cloud lifetime effect*), has generated a need to quantify the magnitude of this effect. So far, however, there exists little direct evidence to support or deny the initial hypothesis. This is hardly surprising given the level of complexity of the processes involved and the lack of adequate control conditions. To simplify the hypothesis, it may be useful to split it conceptually into three separate process hypotheses, each of which must be verified:

H1: Changes in aerosol concentrations result in changes to the cloud droplet size distribution, all other controlling variables being held constant. The simplest change that may occur is that increased aerosol concentrations lead to increased concentrations of cloud droplets and therefore smaller droplets.

H2: The aerosol-induced changes to the cloud droplet size distribution result in changes in the collision-coalescence rates which in turn lead to changes in the precipitation rate. The simplest form of this is that smaller, more numerous cloud droplets suppress coalescence rates, for a fixed liquid water content.

H3: Changes in precipitation rate result in changes in the distribution and/or total amount of liquid water that in turn affects the radiative effects of the cloud.

Verification of **H1**, **H2**, and **H3** is necessary, but not sufficient to determine the climatological significance of the second indirect effect: placing the hypotheses into a quantitative framework is likely to remain a challenge for some time. Evidence supporting **H1** first emerged

in the 1960s (e.g. Twomey and Warner, 1967). A wealth of subsequent observations (Martin et al., 1994; Gultepe et al., 1996; Brenguier et al., 2000; Durkee et al., 2000; Ackerman et al., 2000; Taylor et al., 1999) have confirmed **H1**, although the climatological significance remains uncertain (Haywood and Boucher, 2000) and the relationship between aerosol and cloud droplet number concentration is complex (Gultepe et al., 1996). Differing aerosol size distributions and chemical compositions (Pruppacher and Klett, 1997), updraught speeds (Snider et al., 2002), entrainment (Korolev and Isaac, 2000), radiative growth (Austin et al., 1995a; Harrington et al., 2000), and ripening effects (Celik and Marwitz, 1999; Wood et al., 2002) all complicate this relationship, and need to be better quantified, particularly on the large-scale using satellites (Nakajima et al., 2001; Breon et al., 2002).

There is less evidence for **H2**, probably because drizzle has traditionally been considered a secondary property of MBL clouds, and has not been the primary focus of observational studies. Yum et al. (1998) and Yum and Hudson (2002) show decreasing *drizzle* liquid water contents in stratus as N_d increases. Hudson and Yum (2001) find this to be the case in small cumuli, and Comstock et al. (2003) find a significant negative correlation between drizzle rate and N_d in SE Pacific stratocumulus.

We summarize the current status of evidence for **H2** in Fig. 1 which shows precipitation rate ($R(z_{CB})$, nominally at the cloud base) against N_d for MBL clouds from around the world. Despite considerable spread in the precipitation rates for any given N_d , there is a distinct trend to lower precipitation rate as the cloud droplet concentration increases, supporting **H2**. Evidence for **H2** on the regional to global scale is lacking at present because current satellite radar observations are not sensitive enough to detect the weak returns associated with MBL drizzle. This situation will change, however, with the launch of the Cloudsat mission (Stephens

et al., 2002). Observations of radar reflectivity returns from MBL clouds will need to be converted to physically significant drizzle parameters (i.e. precipitation rate) before they are useful (Comstock et al., 2003; Van Zanten et al., 2004). We examine such important relations in Part II of this study.

An absence of control conditions precludes purely observational evidence for **H3**. There is some evidence suggesting that the degree of adiabaticity of MBL clouds is reduced when the precipitation rate becomes high (Gerber, 1996; Boers and Rotstayn, 2001, see also this study). However, it may be that the presence of drizzle could lead to less adiabatic, but deeper, clouds with the same liquid water path (*LWP*), and so the radiative effects of precipitation are difficult to assess. The hypothesis **H3** is more amenable to study with high resolution large eddy simulations (LES) containing explicit microphysics (Feingold et al., 1997; Khairoutdinov and Kogan, 1999; Stevens et al., 1998). Of these studies, Feingold et al. (1997) and Stevens et al. (1998) demonstrate that in the presence of heavy drizzle, cloud layers have lower integrated water contents, directly supportive of **H3**. There is also no shortage of GCM simulations that demonstrate **H3** (see review of Haywood and Boucher, 2000). However, these simulations necessarily depend upon very simple parameterizations of drizzle production that generally lack validation using observations. We attempt to validate several of the commonly used parameterizations of drizzle production in Part II of this study.

It is now widely acknowledged that considerable spatial variability of cloud *LWP* is the rule rather than the exception (Cahalan et al., 1994; Szczodrak et al., 2001; Wood and Taylor, 2001; Wood and Hartmann, 2003). It is perhaps not surprising, therefore, that recent work has shown that the drizzle in stratocumulus clouds often tends to occur in intermittent localised patches (Austin et al., 1995b; Vali et al., 1998; Stevens et al., 2003; Comstock and Brether-

ton, 2003) rather than being uniformly spread through the cloud. These patches tend to occur in regions where the cloud thickness is locally enhanced. Thicker regions of cloud contain larger cloud droplets and higher liquid water contents near cloud top than thinner regions and the relationship between cloud liquid water content and coalescence rate is strongly nonlinear (Nicholls, 1987; Austin et al., 1995b). Evidence has been presented (Paluch and Lenschow, 1991; Rand, 1995; Jensen et al., 2000) suggesting that the evaporative cooling of drizzle below cloud base may drive mesoscale circulations which affect the thermodynamic and cloud evolution in the MBL (Stevens et al., 1998). We examine the potential coupling between cloud liquid water variability and drizzle variability in this study.

The study comprises two parts. In part I we describe aircraft observations of the horizontal and vertical structure and variability of cloud and drizzle in twelve stratocumulus cloud cases over the NE Atlantic and in UK coastal waters. The clouds examined have a considerable variety of droplet concentrations, *LWP* and drizzle rates which allows us to make inferences about (a) the role of droplet concentration and *LWP* upon the production of drizzle and (b) the effects of drizzle upon the adiabaticity of liquid water content. Aerosol microphysics (i.e. **H1**) are not considered explicitly in this study. Part II of the study presents a more detailed analysis of the size resolved microphysics and the related issues of radar reflectivity-precipitation rate relationships and the parameterization of warm cloud microphysical processes.

Section **2.** presents details of the flights and instrumentation. Section **3.** examines the vertical structure of the cloud and drizzle parameters. Section **4.** describes mesoscale variability of the drizzle, its scaling and intermittency, and Section **5.** examines the timescales involved in drizzle processes. We discuss and attempt to generalize our findings in a discussion, before concluding with suggestions for future work.

2. Case details

a. Flights

Data in this study were collected using *The Met. Office* C-130 aircraft. Twelve flights are presented, with eleven during the day over United Kingdom oceanic waters, and one (A209) at night as part of the ASTEX 1st Lagrangian experiment in NE Atlantic Ocean (Bretherton and Pincus, 1995). The sampling strategy differed between flights, although in each case there was good sampling of the vertical and horizontal structure of the cloud. In all flights the mean aircraft position followed an approximately Lagrangian path, drifting with the mean wind in the MBL. Flights consisted of a series of straight and level runs, in, above and below cloud, together with a number of vertical ascents from above cloud to close to the surface (~ 15 m). Most flights were augmented with a series of porpoise runs up and down through the cloud to improve vertical sampling. Where possible a run close to the surface (~ 30 m) characterised lower boundary conditions. Straight and level runs were typically 60 km in length, but flights A648 and A649 comprised a greater number of shorter runs (20 km).

b. Instrumentation and data analysis methods

The dynamic and thermodynamic measurement system is described in more detail in Rogers et al. (1995). Cloud microphysical measurements were made at 1 Hz using a PMS¹ Forward Scattering Spectrometer Probe (FSSP, Baumgardner et al., 1993) that counts and sizes particles into 15 size bins in the radius range 1-23.5 μm . Larger particles were measured using a PMS 2D-C optical array probe which counts and sizes particles into 32 size bins in the radius range 12.5-400 μm . For the 2D-C data the first size bin is not used as there is large uncertainty

¹Particle Measuring Systems Inc.

in the sizing of particles in this bin (Korolev et al., 1998). Combined FSSP and 2D-C size distributions are produced by linear interpolation in $\log(dN/dr)$ - $\log(r)$ coordinates. Further details of the size resolved microphysics, including sampling issues, and the parameters derived therefrom, are presented in Part II of this study. Turbulent variance and covariance flux measurements were derived from horizontal runs by first detrending the time series using a 3 km wide moving triangular filter and then using eddy correlation.

Sea surface temperature SST is estimated from a run at the lowest flight level using a Heinmann PRT4 radiometer. Ten meter wind speed U_{10} is estimated using the mean wind speed at the lowest flight level and extrapolating this measurement down using a logarithmic wind profile (Bretherton and Pincus, 1995) using a roughness length of 5×10^{-4} m. Friction velocity u_* is estimated using momentum fluxes from the lowest flight leg. Convective velocity scale w_* is estimated using the buoyancy integral method (Nicholls and Leighton, 1986). In some cases the buoyancy integral is negative due to low buoyancy generation in cloud or because the air was being cooled by a lower SST , and in these cases the w_* cannot be defined.

c. Case details and overviews

Table 1 gives details of the dates and locations, together with some mean properties of the clouds measured. Cases are referred to by flight number throughout. There is a considerable range of mean LWP (45 - 360 g m^{-2}), droplet concentration (8 - 420 cm^{-3}) and cloud base precipitation rate (0.054 - 1.12 mm day^{-1}) between flights. Liquid water path is estimated by vertical integration of liquid water content using a number of ascents/descents through the cloud layer. We calculate the mean droplet concentration using all samples in the height range $1/3 < z_* < 2/3$ to avoid sampling regions close to cloud base and cloud top, where z_* is a

normalised height given by

$$z_* = \frac{z - \overline{z_{CB}}}{\overline{z_i} - \overline{z_{CB}}} \quad (1)$$

where $\overline{z_{CB}}$ and $\overline{z_i}$ are the mean cloud base height and cloud top respectively and z is the height of a particular measurement. Because it is not possible to assign a local cloud base to every measurement, it is possible due to the spatial and temporal variability in the cloud geometrical properties that a measurement at height z could be either above or below cloud base when $z_* = 0$. We calculate the cloud base precipitation rate R_{CB} as being the average precipitation rate for $0 < z_* < 1/3$.

Dynamic and thermodynamic parameters are given in Table 2. Turbulent kinetic energy (TKE) in the MBL is generated by buoyant generation, shear generation, or a mixture of the two. In boundary layers driven predominantly by shear generation observations the vertical wind variance scales well with u_* (see e.g. Nicholls and Leighton, 1986) and we find this for cases A644, A648 and A762. A measure of the relative roles of shear and surface buoyancy production of TKE is given by the ratio of the boundary layer depth z_i to the Monin-Obukhov length L_{MO} . Large positive values of $-z_i/L_{MO}$ indicate that turbulence is driven primarily by thermal convection. Small negative values that shear generation of turbulence dominates. Our definition of L_{MO} accounts for the fact that cloud top cooling in addition to surface forcing can be an important source of buoyancy generation, so we define $L_{MO} = -z_i k u_*^3 / w_*^3$ where $k = 0.4$ is the Von Karman constant. Table 2 shows that flights A049, A209, A439, A641, A649, A764 and A767 are all dominated by buoyancy generation, with the other flights being driven primarily by shear.

Mean in-cloud vertical wind standard deviation $\overline{\sigma_w}$ tends to be larger in the convectively driven cases. To assess the role of radiation in generating cloud turbulence we simulate ra-

diative transfer through the clouds using a four-stream radiative code (Edwards and Slingo, 1996). Long-wave flux divergences ΔLW across the boundary layer are all negative (net loss) and range from around -50 W m^{-2} in cases with relative cold cloud tops and moist lower tropospheres, to -85 W m^{-2} in summer cases with low moisture above the boundary layer. Short-wave flux divergences ΔSW depend strongly upon solar zenith angle. Because all of the flights were flown at approximately the same local time each day (apart from A209 which was at night), this results in a strong winter-summer difference in ΔSW , with relatively little absorption for the winter cases (maximum 21 W m^{-2}) to magnitudes comparable to, or even greater than ΔLW for summer cases. For all the winter cases this results in a net radiative energy loss of $30\text{-}45 \text{ W m}^{-2}$. The net gain/loss in the daytime summer cases is much smaller (net losses between -7 to 24 W m^{-2}).

Only two cases had cloud layers that were clearly decoupled from the surface mixed layer (A649 and A767). The reasons for decoupling in A649 (with a mixed layer base at $z \approx 200\text{m}$) are difficult to determine but in A767 a high surface latent heat flux (110 W m^{-2}) was promoting a warming-deepening form of the decoupling (Bretherton and Wyant, 1997) as the air mass had moved southwards from the Arctic over the previous two days. Cumulus clouds were observed to form at the top of the surface mixed layer ($\approx 600\text{m}$) and in places penetrated the overlying stratocumulus layer. The other summer case boundary layers remained coupled.

The clouds and MBL observed in cases A644 and A648 were markedly different in nature to the other cases (which we will refer to throughout as “well-mixed”). Both cases were formed in moist airmasses moving northeastwards from the Azores region over colder seas. Fig. 2 shows profiles for A644. Surface heat fluxes in these cases were negative and a shallow (200 m deep) shear-driven mixed layer was present. Above this layer the temperature exhibited

a stable lapse rate ($2-3 \text{ K km}^{-1}$) up to around 800-1000 m. Patchy layers of cloud were present at most levels in this layer. Above this layer the temperature profiles indicate a moist adiabatic lapse rate which contained less cloud than the stable layer below. This layer was capped with a weak inversion (1-3 K) at 1800-2000 m (A644) and 1400-1600 m (A648) with layer cloud beneath. Back-trajectories suggest that lower tropospheric air underwent large-scale ascent in the 24 hour period prior to the observations taken on flights A644 and A648. This ascent was associated with warm frontal zones which, although the surface fronts were analysed as being at least 100-200 km from the observational areas, appeared to have a marked affect upon the boundary layer. The ascent rates for the 24 hour period prior to the observations were estimated as 0.9 and 0.8 cm s^{-1} for A644 and A648 respectively, although the trajectories suggested no large-scale ascent on A644 during the observational period, and subsidence during the observational period on A648.

The mean in-cloud vertical wind integral scale $\overline{\lambda_w}$ is calculated using the autocorrelation method of Lenschow and Stankov (1986). This is a measure of the horizontal distance over which the vertical wind decorrelates, so that large values indicate that large coherent eddies are dominant. Typically in a convective boundary layer this integral scale tends to be smallest at the surface increasing with height. We find this to be the case here. The integral scale tends to be smallest in clouds capping shallow boundary layers (A693, A763 and A764 all have cloud tops lower than 500 m and $\overline{\lambda_w} < 100$ m) especially in those with shear-driven mixing.

3. Vertical structure

a. Temperature and total water content

Figure 3 shows profiles of liquid potential temperature θ_L and total water content q_T in the cloud layer, referenced to the cloud layer means θ_{L^*} and q_{T^*} . Liquid potential temperature

and total water content in all cases except A644 and A648 are almost constant with height, as one would expect for a well-mixed boundary layer where the entrainment rate is small ($w_e/w_* \ll 1$). The Rosemount E102AL total temperature sensor used on the C-130 measures air temperature with an error of approximately 0.2-0.5 K, which is too large to determine significant deviations from adiabaticity in the “well-mixed” cases except close to cloud top. The deviations in A644 and A648 are significant and highlight the considerable subadiabaticity and poor vertical mixing in these cases.

b. Liquid water content and droplet concentration

To facilitate the comparison between flights we define N_* (Table 1) as the mean in-cloud droplet concentration for each case, with a 1 Hz sample defined as cloudy if the FSSP droplet concentration exceeds 5 cm^{-3} (Wood and Field, 2000). Because the droplet concentrations in A644 and A648 were in places very low ($< 10 \text{ cm}^{-3}$) we use the 1 Hz Johnson-Williams (JW) liquid water content with a threshold of 0.02 g kg^{-1} in these cases. We then calculate layer averages over a number of height bins in the range $0 < z_* < 1$. Figure 4 shows profiles of droplet concentration and cloud liquid water content characteristics for each flight. Cases other than A644 and A648 show similar behaviour with $\overline{N_d}/N_*$ increasing with normalised height up to around $z_*=0.3-0.4$ then remaining approximately constant and unity up to $z_*=0.8$. Above this height the droplet concentrations decrease. It is important to stress that fluctuations in cloud base and cloud top heights are the main cause of the low values close to cloud boundaries. In-cloud means are close to unity from cloud base to $z_* \approx 0.9$. Standard deviations of the droplet concentration at each height normalised with the mean value at that height are found to increase close to the cloud boundaries due to the averaging over both cloudy and clear

regions. In the cloud centre $\sigma_{N_d}/\overline{N_d}$ is typically 0.1-0.4 for the “well mixed” cases, comparable to those presented in Noonkester (1984). In contrast, the cases A644 and A648 show larger values through much of the cloud layer reflecting both the broken nature and possibly the drizzle depletion of droplets in these layers.

The subadiabatic nature is more easily observed using deviations of liquid water content from adiabatic than by looking at temperature or total moisture. We use the same formulation as (Nicholls and Leighton, 1986) in that we define $q_{ad}(z_i)$ as the adiabatic liquid water content at cloud top, i.e. $q_{ad}(z_i) = \Gamma_{ad}(\overline{z_i} - \overline{z_{CB}})$ where $\Gamma_{ad}(T, p)$ is the adiabatic increase in liquid water content with height, a weak function of temperature and pressure. A single value of Γ_{ad} is used in each case, calculated using the mean in-cloud temperature and pressure. We then calculate the degree of subadiabaticity by calculating q_{ad} for each level, subtracting the observed mean value $\overline{q_L}$ and normalising with $q_{ad}(z_i)$. This parameter (Fig. 4(c)) is zero for a fully adiabatic cloud and equal to z_* for cloud free conditions. The clouds range from close to adiabatic (A641) to very subadiabatic (A644, A648) with a broad range in between. Parameters that can affect the adiabaticity are drizzle loss (Stevens et al., 1998) and the balance between the transport of moisture through the cloud boundaries and the efficiency with which turbulent motions can redistribute the moisture through the layer (Wyngaard and Brost, 1984; Nicholls and Leighton, 1986). The normalized standard deviation of the liquid water content typically decreases through the lowest 2/3 of the cloud before increasing again as the upper boundary is reached.

We carried out a more detailed study of the subadiabatic nature of the clouds by considering each profile individually. For each profile we estimate cloud base and top from the droplet concentration measurements. We estimate LWP from the profile by simple vertical integra-

tion of the observed q_L , and the adiabaticity f_{ad} as the ratio of the observed LWP to adiabatic LWP_{ad} cloud liquid water path, since $LWP_{ad} = (1/2)\Gamma_{ad}(z_i - z_{CB})^2$. The mean of these values for each flight is given in Table 3. The uncertainty in mean LWP is estimated using profiles through a hypothetical cloud where the local liquid water content is a linear function of height above the local cloud base. The cloud has a sinusoidal cloud base and flat cloud top, with an amplitude of taken from the different observations of cloud base height. The horizontal wavelength is taken to be 20-40 km, a typical lengthscale for cloud base fluctuations in stratocumulus clouds. Each individual profile can result in a biased LWP because of variations in cloud base. Given enough profiles for each case this method results in an unbiased estimate of the cloud LWP and f_{ad} . The errors increase as the horizontal wavelength increases and decrease as the number of profiles increases. The error in f_{ad} is shown in Table 3. This error does not include unknown systematic errors in the JW liquid water content sensor used to make the measurements, but these are likely to be smaller than 10%.

Figure 5 shows, for two cases, the mean ratio q_L/q_{ad} of observed to adiabatic liquid water content as a function of normalised height using the individual profile method. Both cases show a near-constant value of of adiabaticity through the bulk of the cloud ($0.2 < z_* < 0.9$) with a fall-off, presumably due to entrainment, for $z_* > 0.9$. Values close to cloud base are more prone to error because of the small values of liquid water content there. The results suggest that the cloud in A641 is close to adiabatic and that the liquid water content in A763 is roughly 60-70% of adiabatic. This is reasonably consistent with the values in Fig. 4(c). We are fairly confident about adiabaticity values in most of the clouds (see estimated errors in Table 3), and we examine the possible cause of the variability among the different cases in Section 5.

c. Cloud fraction

Cloud fraction (CF , Figure 6) in the “well-mixed” is close to unity ($CF > 0.9$) in the range $0.3 < z_* < 0.8$ with a drop-off to 0.4-0.8 at mean cloud base and top. For A644 and A648 $CF < 1$ at all levels. The largest CF (0.6-0.8) in these cases is found for $z_* < 0.5$, with minimum coverage at intermediate levels, and a second peak in CF around $z_* = 0.8 - 0.9$. It is interesting that the frontal cases both show considerable similarities with each possessing a two-layer cloud structure. Very low accumulation-mode aerosol concentrations (10-20 cm^{-3}) were observed in the relatively clear between the layers and above cloud in both cases, suggesting that depletion of aerosol through heavy drizzle may be rendering the upper cloud deck colloidally unstable. The lower cloud layer may have resulted from the moistening and cooling of the boundary layer caused by evaporating drizzle from the upper level. The two-layer structure observed in both frontal cases may be a common feature of marine stratus in near-frontal warm sectors.

d. Vertical wind

Vertical wind standard deviation σ_w is a signature of turbulent mixing in the cloud, and σ_w (Fig. 7(a)) is relatively independent of height in the buoyancy-driven cases. Shear-driven cases (particularly A644 and A648) show a general decrease in σ_w with height reflecting that the turbulence is driven primarily by surface friction. The vertical wind integral scale λ_w , varies considerably between cases, and with height in some of the cases (Fig. 7(b)). As noted in Section 2. c. shear-driven turbulence generally results in smaller eddies. Lenschow and Stankov (1986) find that in convective boundary layers driven by surface heating the integral scale increases with height away from the surface. Clearly it seems intuitive to find eddy sizes

becoming smaller towards fixed boundaries. However, for turbulence generated near cloud top as in the case of radiatively driven stratocumulus, the inversion does not impose a rigid lid to the turbulent eddies, but it dampens considerably the larger eddies leading to smaller integral scales. However, gravity waves that may occur in the stable inversion layer cannot easily be distinguished from turbulent eddies in autocorrelation, and it is unclear what one should expect. Our results do not appear to show any consistent height trends in the integral scale. The integral scale is an important constraint upon simulations of the effect of turbulence on drizzle (Austin et al., 1995b; Baker, 1993) because it is related to the Lagrangian eddy timescale that, with σ_w , determines the redistribution of drizzle drops in the MBL, which controls the growth of the largest drizzle drops.

e. Drizzle bulk microphysics

Drizzle drops, in this study defined as drops with radii larger than $20 \mu\text{m}$, were present in all cases. We choose $20 \mu\text{m}$ as a partition because it represents the crossover radius where coalescence becomes more effective than condensation (e.g. Jonas, 1996). Observations of cloud droplet ($r < 20\mu\text{m}$) size distributions in warm stratiform cloud are quite common in the literature (e.g. Noonkester, 1984; Nicholls, 1984; Liu and Hallett, 1998; Boers et al., 1996; Martin et al., 1994; Brenguier et al., 2000; Wood, 2000). A much smaller number of studies exist that focus upon drizzle microphysics (e.g. Nicholls, 1987; Boers et al., 1996; Wood, 2000).

Figure 8 shows characteristics of the populations of drizzle droplets ($r > 20\mu\text{m}$) at different levels in cloud. Drizzle droplet concentrations $N_{d,D}$, liquid water contents $q_{L,D}$ and precipitation rates R are all normalised with their respective in-cloud means, given in Table 4.

For “well-mixed” cases, drizzle drop concentrations are roughly constant throughout the upper 40% of the cloud and decrease at lower levels. This demonstrates that the initial source of the drizzle drops is close to the top of the cloud, where the highest liquid water contents and largest cloud droplets are. In general, observations of drizzle in stratocumulus clouds show that the drizzle droplet size distributions broaden towards clouds base. This is because drizzle drops form in the upper levels of the cloud through the coalescence of cloud drops (autoconversion). These drops then fall through cloud growing larger by collecting cloud (accretion) and drizzle (self-collection) drops. Fig. 8b shows that indeed the drizzle drop size, presented here in the form of the volume radius, increases downward through the cloud. Drizzle liquid water contents (Fig. 8c) are roughly constant through the cloud and decrease only at its extremities. Precipitation rates (Fig. 8d) are roughly constant through the lowest two-thirds of the cloud and decrease above this quite markedly. This is evidence that although most of the drizzle drops are created close to the top of the cloud through autoconversion of cloud droplets, the larger drops that dominate the precipitation rate are generated further down in the cloud (see part II of this study).

f. Moisture transport

Vertical turbulent fluxes of total water content $\overline{wq_T}$ are compared with the precipitation rate in Fig. 9. No flux data are available from A049 or A439. In most of the well mixed cases there is a general balance indicating that removal of moisture by gravitational settling of drizzle drops is approximately balanced by a corresponding moisture flux, as previously observed in the ASTEX 1st Lagrangian case (de Roode and Duijkerke, 1997). In several cases the moisture fluxes exceed the precipitation fluxes. In the two heterogeneous cases (A644 and

A648), the turbulent moisture fluxes are small, and in A644 actually negative, throughout the cloud, indicating that drizzle in these cases is depleting cloud water. In A644 and A648, it is estimated that complete removal of the upper layers of cloud would take place in under two hours if the precipitation and turbulent moisture flux remains unchanged. This may be an example of a general transition from a deep cloud-filled near-frontal layer to a more shallow MBL.

g. Sub-cloud microphysics

Removal of cloud liquid water by drizzle and its subsequent evaporation below cloud base leads to a heat source/moisture sink in the cloud layer and a heat sink/moisture source below it. The evaporation rate profile is therefore crucial. A simple model of the sedimentation-evaporation process is constructed to describe the evolution of a population of drizzle drops falling and evaporating below cloud base (Comstock et al., 2003). Solutions are obtained for the temperature range 270-290 K and for cloud base $r > 20\mu\text{m}$ volume radii $r_{v,D(CB)}$ from 30-80 μm , covering the range of observations. Profiles of temperature and moisture below cloud base are assumed to be adiabatic. A parameterization described in Comstock et al. (2003) is derived from the model, and the profile of precipitation rate normalized with its cloud base value depends strongly upon $r_{v,D(CB)}$. Figure 10 indicates that the model parameterization represents a good fit to the observations.

As a general rule, approximately 50% of the drizzle flux in the cases studied here evaporates within 60-100 m of cloud base and 80% within 150-250 m of cloud base. This is likely to be a general result for drizzling stratocumulus, and is supported by observations in the SE Pacific (Bretherton et al., 2004). It is therefore more likely that drizzle will affect turbulent

dynamics through moistening and cooling of the subcloud layer than by removal of moisture to the surface, except in cases with very low cloud base.

Evaporative cooling rates (per mm day⁻¹ R_{CB}) from the model as a function of height and $r_{v,D(CB)}$ (Fig. 11) can be as large as the LW radiative cooling rate which is usually 4-10 K day⁻¹ averaged over the depth of the MBL. For $R_{CB} = 1$ mm day⁻¹ and $r_{v,D(CB)} = 40$ μm , peak subcloud cooling rates are around 12 K day⁻¹ at around 100 m below cloud base. The cooling rate averaged over the 300 m deep layer below cloud base is 7.6 K day⁻¹.

4. Horizontal variability

Drizzle tends to occur in intermittent and localised structures, rather than being evenly distributed (Austin et al., 1995b; Stevens et al., 2003; Comstock et al., 2003; Comstock and Bretherton, 2003). Systematic quantitative analysis of the variability has not been the focus of previous studies, and yet such variability may play a central role in drizzle processes. How is drizzle production related to the spatial variability in cloud structure? In this section we focus upon aspects of the drizzle spatial variability using a number of techniques.

a. Subcloud temperature and humidity variability

Horizontal runs below cloud reveal large variability in the virtual potential temperature and specific humidity on scales larger than 1 km. Several authors have reported measurable cooling and moistening of the subcloud layer on $>$ km scales, associated with the evaporation of drizzle (Paluch and Lenschow, 1991; Jensen et al., 2000). Here, we separate subcloud runs into drizzling and non-drizzling regions (using a threshold $R = 0.01$ mm day⁻¹). Time series of 10-second means are used to examine scales $>$ 1 km. We calculate the mean virtual potential temperature θ_v and total water q_T for the drizzle and drizzle-free regions. For all sub-

cloud runs containing 20-80% drizzle points, we plot the θ_v difference between drizzle and the drizzle-free regions against the corresponding q_T difference (Fig. 12). For evaporating drizzle, assuming constant background conditions between the drizzle and drizzle free regions, cooling and moistening are coupled. Two cases (A209 and A049) show good coupling. In most other cases the difference in specific humidity is larger than that expected for evaporation alone. Interestingly, the drizzle regions are almost universally cooler and moister than the drizzle-free regions. With relative cooling in drizzle regions being 0.1-0.4 K, this is highly suggestive of a possible evaporative dynamic feedback.

b. Sizes of drizzle patches

Vali et al. (1998) presented some of the first radar observations of drizzle spatial variability in marine stratus clouds. They found, in their three cases, regions of high radar reflectivity organised into cells with a dominant spacing of 1.2-1.5 times the depth of the cloud layer, but that the cells occur in a wide range of sizes. We use data from horizontal runs (20-100 km in length) to examine drizzle cell size using the 2D-C probe. We use the 10 s (1 km horizontal scale) precipitation rate series and identify regions for which the precipitation rate is larger than the median value for the run. This allows a separation into regions of less and more intense precipitation, while maintaining good statistics. Around 95% of these regions are smaller than 10 km and so the analysis is not too badly limited for the shorter runs, although there is of course a tendency to underpredict the mean cell size in these cases. A repeat of the analysis with only runs longer than 60 km revealed little qualitative difference in the distribution of cell sizes. Changing the drizzle threshold also made little difference to the results.

Runs are subdivided into in-cloud and subcloud. Cumulative distributions of cell sizes

for all flights (Fig. 13) have several interesting features. First, drizzle cell sizes are typically small with approximately 90% smaller than 8 km both in and below the cloud. The median cell sizes are 2-3 km. For the in-cloud data, over 99% of cells are smaller than 20 km. These facts demonstrate that drizzle production is highly localised, rather than being spread evenly through the cloud. Second, below cloud, larger cells are more common than they are in the cloud. Cells larger than 15 km are 2-3 times more common below cloud, and this difference increases as the cell size increases. Sampling is poor above 20 km and so it is difficult to make quantitative inferences concerning the largest cells. The mean cell size for each flight ranges from 2.4 to 4.7 km. The frequency distribution of cell sizes is largest at 1 km suggesting that higher resolution observations would yield a considerable fraction of cells with sub 1 km scale. This may be why our values are somewhat larger than those found by Vali et al. (1998) using aircraft radar with high spatial resolution.

c. Power spectra and structure functions

A composite power spectrum of precipitation rate is derived from all the level runs in and below cloud (Fig. 14). Although there is considerable noise in the spectral estimates, it is clear that the power spectrum follows an approximate power law relation from the smallest scales (2 km) to several tens of km. There are examples in the literature showing power law scaling in this range for liquid water content or path (e.g. Cahalan and Snider, 1989; Davis et al., 1996), and cloud base height (Wood and Taylor, 2001). However, as far as the author is aware, this is the first example of power law scaling in precipitation rates found in drizzling MBL clouds. Importantly, the magnitude of the power law exponent β here is much lower than those found for *LWP*, having a value $\beta = 1.16 \pm 0.1$ ($2\text{-}\sigma$ level). This demonstrates heightened variability

in drizzle at small scales.

Structure functions (Davis et al., 1996) are complementary to spectral analysis, and we examine the statistical properties of the increments at scale r , namely $\Delta R(r; x) = R(x+r) - R(x)$, $0 \leq r \leq L$, where L is the length of the spatial series. Over the scale invariant range (1-20 km), we derive the function $\zeta(q)$, defined by

$$\langle |\Delta R(r)|^q \rangle \propto r^{\zeta(q)}, \quad q \geq 0, \quad (2)$$

with $\langle \rangle$ being an ensemble average. A measure of the stationarity in the series is provided by $H(q) = \zeta(q)/q$. We use $H_1 = \zeta(1)$ to characterize the stationarity in the precipitation rate. We find that $H_1 = 0.12$ and $H_2 = 0.09$ for the in-cloud data. The Weiner-Khinchine theorem Monin and Yaglom (1975) gives $\beta = 2H(2) + 1$, so the spectral and structure function analyses show consistency. The results indicate that the precipitation rate is more stationary than the cloud liquid water ($H_1 = 0.28 - 0.29$ for cloud liquid water content fields, Marshak et al. 1997).

d. Intermittency

Singular measures (Marshak et al., 1994; Davis et al., 1994, 1996) are used to characterize intermittency in the the precipitation. Again, we use long (>30 km) straight and level runs and pad out the data with zeros to give a series with a length equal to an integral power of two. The padding does not seriously affect the resulting intermittency measure, for which we use:

$$\epsilon(\eta; x) = \frac{|\Delta R(\eta; x)|}{|\langle \Delta R(\eta; x) \rangle|}, \quad 0 \leq x < L - \eta, \quad (3)$$

where $\Delta R(\eta; x)$ is the η -scale precipitation rate gradient field $R(x)$, and L is the length of the series. We focus upon coarse-grained versions of the gradient field which we consider as a

function of the scales $r(\eta < r \leq L)$ over which we perform spatial averaging

$$\epsilon(r; x) = \frac{1}{r} \int_x^{x+r} \epsilon(\eta; x') dx', \quad \eta \leq x \leq L - r. \quad (4)$$

We find that the measures $\langle \epsilon(r)^q \rangle \propto r^{-K(q)}$, $q \geq 0$, i.e. they are described well as power laws over some range of scales r (here, from 1 km to ~ 10 -20 km). Finally, we define $C_1 = K'(1)$, which takes values between 0 and 1, as a measure of the intermittency in the field $R(x)$ (e.g. see examples and further details in Davis et al. 1994).

Davis et al. (1996) analyzed the intermittency in liquid water content in stratocumulus clouds and found $C_1 \approx 0.08 - 0.10$. For precipitation rate in our cases we find that values of C_1 are much larger than for the cloud liquid water, with median C_1 values of 0.15 and 0.18 for in-cloud and below-cloud data respectively. Further partition shows that C_1 decreases upwards through the cloud, with C_1 in the lower half of the cloud layer being similar to that in the subcloud layer. We find that C_1 is quite well parameterized as a function of $\gamma_R = (\overline{R}/\sigma_R)^2$, such that $C \propto (1/\gamma_R)^{1/2}$.

e. Drizzle in the mean multifractal plane

Davis et al. (1994) and Marshak et al. (1997) introduce the *mean multifractal plane* as a formalism to characterize the multifractal properties of geophysical fields. The two axes of the plane correspond to H_1 , the degree of non-stationarity/smoothness and C_1 , the degree of intermittency. Precipitation fields in drizzling MBL clouds are more stationary but more intermittent than cloud liquid water content (Fig. 15), with C_1 closer to values found in turbulent velocity and dissipation fields (Schmitt et al., 1992). Data from several field projects are shown. Cloud liquid water content and *LWP* fields tend to group together with H_1, C_1 pairs of [0.25-0.35, 0.07-0.12]. Precipitation rate fields from this study and from drizzling stratocumulus

during EPIC (East Pacific Investigation of Climate, Bretherton et al. 2004) also group together with $H_1 \approx 0.1$ and $C_1 \approx 0.2$. Such consistent behavior requires explanation.

f. Links between LWP and drizzle variability

Given that cloud water is the source of the precipitation, one is compelled to ask why statistical properties of the cloud and drizzle fields are so distinct. We hypothesize that enhanced intermittency in precipitation compared with cloud water is indicative of a nonlinear relationship in the conversion rate of cloud liquid water to precipitation (see also part II of this study). Figure 4 shows that, in the bulk of the cloud, the relative degree of spatial variability in cloud liquid water content is generally somewhat larger than the variability in cloud droplet concentration. Figure 16 suggests that the drizzle rate variability is indeed quite well correlated with the degree of variability in cloud *LWP*, and that droplet concentration, in general is less variable. The more accurate autoconversion schemes (see Part II) have a greater dependence upon liquid water content than droplet concentration. It seems reasonable to posit that drizzle production is more strongly modulated by liquid water content than by droplet concentration.

Assuming, for simplicity, that the sole modulator of precipitation rate is cloud liquid water, we find that fields with intermittency and stationarity properties typical of precipitation rate can be obtained from fields of *LWP*, where $y = LWP^\eta$, with η being a tunable parameter. One dimensional *LWP* fields with the observed mean multifractal properties (here, set constant with $H_1 = 0.3$ and $C_1 = 0.1$ are constructed using a bounded cascade model (Marshak et al., 1994). Each value of η leads to different mean multifractal properties of the simulated y field. Figure 17 shows values of H_1 and C_1 as a function of η for the simulated fields. For $3.5 < \eta < 4.5$, the derived fields y have H_1 and C_1 characteristic of observed drizzle precipitation.

Although this result is by no means proof of a direct link between cloud and precipitation structure, it suggests that a strongly nonlinear dependence of precipitation generation upon cloud water can account for the spatial variability characteristics of precipitation in stratiform boundary layer clouds. Such a nonlinear dependence is consistent also with microphysical results presented in part II of this study.

5. Drizzle timescales

The time required for the complete removal of all cloud water through rainout, assuming a constant cloud-base precipitation rate R_{CB} , is $\tau_{driz} = LWP/R_{CB}$. For the clouds studied here (see Table 1), this rainout timescale τ_{driz} varies from 1.8 hr (A644) to 160 hr (A641). Cloud liquid water is replenished through turbulent fluxes for which we define a timescale τ_{rep} . We might expect τ_{rep} to scale with the eddy turnover timescale, here defined as $\tau_w = z_i/\overline{\sigma_w}$. We introduce a simple equilibrium model of drizzle production where the loss of cloud water path through precipitation at cloud base R_{CB} is balanced by a turbulent replenishment that relaxes the cloud LWP back to the adiabatic value LWP_{ad} with a timescale τ_{rep} :

$$\frac{d(LWP)}{dt} = \frac{LWP_{ad} - LWP}{\tau_{rep}} - R_{CB} = \frac{LWP_{ad} - LWP}{\tau_{rep}} - \frac{LWP}{\tau_{driz}}. \quad (5)$$

In equilibrium $d(LWP)/dt = 0$, so we can rearrange (5), with the definition of adiabaticity $f_{ad} = LWP/LWP_{ad}$ to give

$$f_{ad} = (1 + \tau_{rep}/\tau_{driz})^{-1} \quad (6)$$

When $\tau_{rep}/\tau_{driz} \ll 1$, drizzle processes should not have a significant effect upon cloud adiabaticity. We do not know the value of τ_{rep} but we might expect it to scale with the eddy

turnover timescale τ_w . Figure 18 shows the adiabaticity f_{ad} of the clouds plotted as a function of τ_w/τ_{driz} . When $\tau_w/\tau_{driz} > 0.01 - 0.02$, the clouds have markedly sub-adiabatic liquid water contents. Drizzle is not the only process, however, that can affect f_{ad} . Nicholls and Leighton (1986) estimate that a value of $f_{ad} = 0.8$ is a reasonable estimate of the adiabaticity due to entrainment processes. This may be overestimate the effects of entrainment however, because several of the clouds studied in Nicholls and Leighton (1986) were drizzling, and some of the subadiabaticity observed may have been related to depletion by precipitation processes rather than by entrainment. In case A641 (greatest τ_{driz}), $f_{ad} \approx 1$, although we would expect this cloud to be entraining considerably based upon w_* and $\Delta\theta_v$ (Table 2). However, we might also expect the effects of entrainment upon cloud liquid water content in this case to be limited because the air was very moist above the boundary layer. Assuming that drizzle is a dominant cause of subadiabaticity in our clouds, we find $f_{ad} \sim 0.5$ when $\tau_{driz} \sim 0.1 - 0.5\tau_w$ (Fig. 18). This implies that in most cases the replenishment timescale is considerably longer (2-10 times) than the eddy turnover timescale.

The replenishment timescale may be linked more closely with the development of the observed mesoscale drizzle cells rather than eddies with sizes comparable with z_i . Certainly, our power spectral observations show that the drizzle organisation is not confined to horizontal scales comparable with the boundary layer depth, and extends to scales of tens of kilometers, with mesoscale temperature variations of a few tenths of a K . The propagation speed U of a density current of depth h can be estimated from $U = \sqrt{gh\Delta\theta/\theta}$ (e.g. Simpson, 1997), with $\Delta\theta$ being the potential temperature deficit in the advancing cold current. For $\Delta\theta = 0.2 - 0.5$ K and $h = 300 - 500$ m (\sim the subcloud layer depth), this gives $U \approx 1.5 - 3$ m s⁻¹. Observed mesoscale wind variations are comparable to this (not shown). For cells with horizontal scales

of the order of 10-30 km, the timescale for a mesoscale cellular circulation is several times longer than the eddy turnover timescale, and may explain why the clouds have lower f_{ad} than might be expected if cloud liquid water is replenished on a timescale τ_w .

6. Discussion and conclusions

Aircraft observations of twelve stratiform MBL clouds have been presented to investigate aspects of drizzle, paying particular attention to vertical and horizontal variability. Normalized variables were used where possible to facilitate comparison. The cases separate into two broad types. Ten of the cases are unbroken, quite well mixed, and display many common properties. Briefly summarized, the common properties are:

- (a) almost constant liquid potential temperature and total water content in the cloud layer, and linear (although mainly subadiabatic) increase in liquid water content with height;
- (b) near-constant cloud droplet concentration with height;
- (c) minima in normalized standard deviations ($\sigma_x/\bar{x} \approx 0.2 - 0.4$) of droplet concentration and liquid water content in the center of the cloud, with maxima ($\sigma_x/\bar{x} \approx 1 - 1.5$) close to cloud boundaries;
- (d) vertical velocity standard deviations are $0.25-0.75 \text{ m s}^{-1}$ throughout the cloud layer with no major height variation;
- (e) relatively constant drizzle drop concentrations ($r > 20\mu\text{m}$) in the upper 40% of the cloud and decreasing below this, with drizzle drop volume radius increasing downward from $25-35 \mu\text{m}$ near top to $40-60 \mu\text{m}$ at the base;
- (f) drizzle liquid water contents constitute only a small fraction ($< 10\%$) of the total condensed water;
- (g) precipitation rate is near-constant in the lowest 60% of the cloud and decreases above this height.

The findings are consistent with an initial production of drizzle drops near cloud top, where liquid water contents are largest. Precipitation rates increase markedly below this due to accretion processes. We explore in more detail the relative contributions of autoconversion and accretion in part II. In contrast to the “well mixed” cases, two of the cases are more heterogeneous, with multiple layers, and are associated with near-frontal warm sectors. These cases

have strong winds, vertical wind variances that decrease upward from the surface, and probably contain some wave activity. These clouds are conditionally stable and total water decreases with height. Liquid water contents are markedly subadiabatic, and drizzle is prevalent throughout. Cloud droplet concentration decreases with height, probably due to the weaker turbulence at higher levels and because cloud condensation nuclei (CCN) are being removed from these levels by precipitation. Cloud properties are considerably more variable in the upper layers. We hypothesize that these clouds may be representative of the transition from a deep, near-frontal cloud layer to a shallow subsidence-dominated MBL, and that precipitation and CCN removal may be important in driving this transition.

Evaporation of drizzle below cloud base is broadly consistent with the results from a simple sedimentation-evaporation microphysical model, which allows a parameterization of the evaporative cooling profile to be constructed that depends only upon cloud base precipitation rate and drizzle drop volume radius $r_{v,D(CB)}$. For values of $r_{v,D(CB)} < 50\mu\text{m}$ the cooling rate has a relatively sharp peak within 100 m of cloud base, with a strong decrease below this. For larger values of $r_{v,D(CB)}$ the evaporative cooling extends over a rather deeper layer and does not have the sharp peak close to the cloud base. The former could lead to a destabilization of the subcloud layer (although still an overall stabilization of this layer with regard to the entire mixed layer). The profile of evaporative cooling, rather than simply the integrated value, could be important in determining the propensity for decoupling, and should be parameterized accurately. Currently adopted forms for evaporation rate profiles in these models (e.g. Turton and Nicholls, 1987; Liou and Ou, 1989) tend to be linear. The sedimentation-evaporation model (Comstock et al., 2003) suggests that an exponential form is more appropriate, and a mixed layer model (Caldwell et al., 2003) suggests that decoupling is sensitive to the shape of the

evaporation rate profile

Spatial variability is of particular importance. First, the mesoscale variability occurs on horizontal scales that are smaller than the current state of the art general circulation model, and must therefore be parameterized (e.g. Cahalan et al., 1994; Oreopoulos and Davies, 1998; Pincus and Klein, 2000; Rotstayn, 2000; Larson et al., 2001; Wood et al., 2002). Second, the mesoscale dynamics of boundary layer systems, and particularly the role of precipitation, is poorly understood. In this study we examine aspects of the horizontal variability. First, we show that in the subcloud layer, regions containing drizzle are generally cooler and more moist than drizzle-free regions, which is suggestive of evaporative cooling. Such mesoscale θ_v (up to 0.5 K) and moisture (up to 0.3 g kg^{-1}) variations may drive mesoscale circulations, as suggested in the conceptual model of Rand (1995). This mesoscale anti-correlation between temperature and moisture is also seen in cross-spectral analysis in regions dominated by boundary layer cloud (Wood and Taylor, 2001). The precipitation rate exhibits scale invariance, from the smallest scale (here restricted to 2 km due to sampling limitations) up to several tens of km. The scaling is quite robust in the ensemble, although sampling limitations precluded a case-by-case analysis. The power spectral scaling exponent ($\beta = 1.16 \pm 0.10$) is much lower than is observed in several other cloud parameters such as liquid water content ($\beta = 1.36 - 1.43$, Davis et al. (1996)), saturation deficit/excess (implied $\beta = 1.65$, Wood et al. (2002)), optical thickness (β close to $5/3$, Cahalan and Snider (1989)), and LWP ($\beta = 1.51$, Wood and Taylor (2001)), indicating that precipitation rate exhibits relatively higher fluctuations on smaller scales than other cloud-related variables. This can be explained by a strongly nonlinear dependence of autoconversion rate upon cloud liquid water content.

The adiabaticity $f_{ad} = LWP/LWP_{ad}$ of the clouds in this study was found to decrease as

the ratio of the eddy turnover timescale $\tau_w = z_i/\overline{\sigma_w}$ to drizzle timescale $\tau_{driz} = LWP/R_{CB}$ increases. A simple equilibrium model of drizzle loss and turbulent replenishment leads to a relationship between f_{ad} and τ_{rep}/τ_{driz} that suggests replenishment of cloud liquid water in MBL clouds occurs on timescales significantly longer than τ_w . This may be indicative of an important role for mesoscale circulations in drizzling MBL clouds.

Recent observations of nocturnal subtropical stratocumulus off the coast of California, Van Zanten et al. (2004) show a remarkably good relationship between mean cloud base precipitation rate, estimated using an airborne millimeter radar, the cloud thickness h , and the cloud droplet concentration N_d , such that $R_{CB} \propto h^3/N_d$. Comstock et al. (2003) also find a good scaling in SE Pacific stratocumulus, with $R_{CB} \propto (LWP/N_d)^{1.75}$, implying a dependence upon $h^{3.5}$ assuming adiabatic clouds. Clouds in this study do not scale particularly well with either of these relationships (Fig. 19). This may be partly a result of poorer estimation of R_{CB} in our cases, perhaps resulting from the lack of a radar to quantify drizzle. However, our study encompasses a wider range of different cloud types (from stratus, to deep stratocumulus, to frontally-influenced stratus), boundary layer depths, and turbulent eddy strengths and sizes. These differences are partly the result of a large range of radiative and dynamical forcing conditions for the clouds in our study compared to the relatively constant forcing in subtropical stratocumulus regions, and might be responsible for the poor precipitation rate scaling of the clouds in this study.

Acknowledgement The author wishes to thank the staff of the Meteorological Research Flight and the C-130 aircrew and groundcrew for their dedication to collecting the data presented in this study. I am grateful to colleagues in the Met Office and elsewhere, for discussions which

aided the research presented in this paper.

References

- Ackerman, A. S., O. B. Toon, J. P. Taylor, D. W. Johnson, P. V. Hobbs, and R. J. Ferek: 2000, Effects of aerosols on cloud albedo: evaluation of twomey's parameterization of cloud susceptibility using measurements of ship tracks. *Bull. Amer. Meteorol. Soc.*, **54**, 1004–1012.
- Albrecht, B. A.: 1989, Aerosols, cloud microphysics, and fractional cloudiness. *Science*, **245**, 1227–1230.
- Austin, P., S. Siems, and Y. Wang: 1995a, Constraints on droplet growth in radiatively cooled stratocumulus clouds. *J. Geophys. Res.*, **100**, 14231–14242.
- Austin, P., Y. Wang, R. Pincus, and V. Kujala: 1995b, Precipitation in stratocumulus clouds: observations and modelling results. *J. Atmos. Sci.*, **52**, 2329–2352.
- Baker, M. B.: 1993, Variability in concentrations of cloud condensation nuclei in the marine cloud-topped boundary layer. *Tellus*, **45B**, 458–472.
- Baumgardner, D., B. Baker, and K. Weaver: 1993, A technique for measurement of cloud structure on centimeter scales. *J. Atmos. Oceanic Technol.*, **10**, 557–565.
- Boers, R., J. B. Jensen, P. B. Krummel, and H. Gerber: 1996, Microphysical and short-wave radiative structure of wintertime stratocumulus clouds over the southern ocean. *Quart. J. Roy. Meteorol. Soc.*, **122**, 1307–1339.
- Boers, R. and L. D. Rotstajn: 2001, Possible links between cloud optical depth and effective radius in remote sensing observations. *Quart. J. Roy. Meteorol. Soc.*, **127**, 2367–2384.

- Brenguier, J. L., P. Y. Chuang, Y. Fouquart, D. W. Johnson, F. Parol, H. Pawlowska, J. Pelon, L. Schuller, F. Schroder, and J. Snider: 2000, An overview of the ace-2 cloudycolumn closure experiment. *Tellus*, **52B**, 815–827.
- Breon, F.-M., D. Tanre, and S. Generoso: 2002, Aerosol effect on cloud droplet size monitored from space. *Science*, **295**, 834–837.
- Bretherton, C. S. and R. Pincus: 1995, Cloudiness and marine boundary layer dynamics in the astex lagrangian experiments. Part i: Synoptic setting and vertical structure. *J. Atmos. Sci.*, **52**, 2707–2723.
- Bretherton, C. S., T. Uttal, . Fairall, C. W., . Yuter, S. E., . Weller, R. A., . Baumgardner, D., . Comstock, K., and R. Wood: 2004, The EPIC 2001 stratocumulus study. *Bull. Am. Meteorol. Soc.*, in press.
- Bretherton, C. S. and M. C. Wyant: 1997, Moisture transport, lower-tropospheric stability, and decoupling of cloud-topped boundary layers. *J. Atmos. Sci.*, **54**, 148–167.
- Cahalan, R. F., W. Ridgway, W. J. Wiscombe, T. L. Bell, and J. B. Snider: 1994, The albedo of fractal stratocumulus clouds. *J. Atmos. Sci.*, **51**, 2434–2455.
- Cahalan, R. F. and J. B. Snider: 1989, Marine stratocumulus structure. *Rem. Sens. Environ.*, **28**, 95–107.
- Caldwell, P., R. Wood, and C. S. Bretherton: 2003, The diurnal cycle of marine stratocumulus in the se pacifi c in a mixed layer context. *J. Atmos. Sci.*, in preparation.
- Celik, F. and J. D. Marwitz: 1999, Droplet spectra broadening by the ripening process. Part i: Roles of curvature and salinity of cloud droplets. *J. Atmos. Sci.*, **56**, 3091–3105.

- Comstock, K. and C. S. Bretherton: 2003, Mesoscale variability of precipitation in stratocumulus. *J. Atmos. Sci.*, in preparation.
- Comstock, K., S. Yuter, and R. Wood: 2003, Radar observations of precipitation in and below stratocumulus clouds. *Quart. J. Roy. Meteorol. Soc.*, in review.
- Davis, A., A. Marshak, W. Wiscombe, and R. Cahalan: 1994, Multifractal characterizations of nonstationarity and intermittency in geophysical fields. *J. Geophys. Res.*, **99**, 8055–8072.
- 1996, Scale invariance of liquid water distributions in marine stratocumulus. Part 1: Spectral properties and stationarity issues. *J. Atmos. Sci.*, **53**, 1538–1558.
- de Roode, S. R. and P. G. Duynkerke: 1997, Observed lagrangian transition of stratocumulus into cumulus during a storm: mean state and turbulence structure. *J. Atmos. Sci.*, **54**, 2157–2173.
- Durkee, P. A., K. J. Noone, R. J. Ferek, D. W. Johnson, J. P. Taylor, T. J. Garrett, P. V. Hobbs, J. G. Hudson, C. S. Bretherton, G. Innis, G. M. Frick, W. A. Hoppel, C. . O’Dowd, L. M. Russell, R. Gasparovic, K. E. Nielsen, E. Ostrom, S. R. Osborne, R. C. Flagan, J. H. Seinfeld, and H. Rand: 2000, The impact of ship-produced aerosols on the microphysical characteristics of warm stratocumulus clouds: A test of mast hypotheses 1.1a and 1.1b. *J. Atmos. Sci.*.
- Edwards, J. M. and A. Slingo: 1996, Studies with a flexible new radiation code. i: Choosing a configuration for a large-scale model. *Quart. J. Roy. Meteorol. Soc.*, **122**, 689–720.
- Feingold, G., R. Boers, B. Stevens, and W. R. Cotton: 1997, A modeling study of the effect of drizzle on cloud optical depth and susceptibility. *J. Geophys. Res.*, **102**, 13527–13534.

- Feingold, G., B. Stevens, W. R. Cotton, and A. S. Frisch: 1996, On the relationship between drop in-cloud residence time and drizzle production in stratocumulus clouds. *J. Atmos. Sci.*, **53**, 1108–1112.
- Gerber, H.: 1996, Microphysics of marine stratocumulus with two drizzle modes. *J. Atmos. Sci.*, **53**, 1649–1662.
- Gultepe, I., G. A. Isaac, W. R. Leitch, and C. M. Banic: 1996, Parameterizations of marine stratus microphysics based on in situ observations: implications for gcms. *J. Clim.*, **9**, 345–357.
- Harrington, J. Y., G. Feingold, and W. R. Cotton: 2000, Radiative impacts on the growth of a population of drops within simulated summertime arctic stratus. *J. Atmos. Sci.*, **57**, 766–785.
- Haywood, J. M. and O. Boucher: 2000, Estimates of the direct and indirect radiative forcing due to tropospheric aerosols: A review. *Rev. Geophys.*, **38**, 513–543.
- Hudson, J. G. and S. S. Yum: 2001, Maritime-continental drizzle contrasts in small cumuli. *J. Atmos. Sci.*, **58**, 915–926.
- Jensen, J. B., S. Lee, P. B. Krummel, J. Katzfey, and D. Gogoasa: 2000, Precipitation in marine cumulus and stratocumulus. Part i: Thermodynamic and dynamic observations of closed cell circulations and cumulus bands. *Atmos. Res.*, **54**, 117–155.
- Jonas, P. R.: 1996, Turbulence and cloud microphysics. *Atmos. Res.*, **40**, 283–306.
- Khairoutdinov, M. and Y. Kogan: 1999, A large-eddy simulation model with explicit microphysics: Validation against aircraft observations of a stratocumulus-topped boundary layer. *J. Atmos. Sci.*, **56**, 2115–2131.

- Korolev, A. V. and G. A. Isaac: 2000, Drop growth due to high supersaturation caused by isobaric mixing. *J. Atmos. Sci.*, **57**, 1675–1685.
- Korolev, A. V., J. W. Strapp, and G. A. Isaac: 1998, Evaluation of the accuracy of pms optical array probes. *J. Atmos. Oceanic Technol.*, **15**, 708–720.
- Larson, V. E., R. Wood, P. R. Field, J.-C. Golaz, T. H. Vonder Haar, and W. R. Cotton: 2001, Systematic biases in the microphysics and thermodynamics of numerical models that ignore subgrid-scale variability. *J. Atmos. Sci.*, **58**, 1117–1128.
- Lenschow, D. H. and B. B. Stankov: 1986, Length scales in the convective boundary layer. *J. Atmos. Sci.*, **43**, 1190–1209.
- Liou, K. N. and S. C. Ou: 1989, The role of cloud microphysical processes in climate: An assessment from a one-dimensional perspective. *J. Geophys. Res.*, **94**, 8599–8607.
- Liu, Y. and J. Hallett: 1998, On size distributions of cloud droplets growing by condensation: a new conceptual model. *J. Atmos. Sci.*, **55**, 527–536.
- Marshak, A., A. Davis, R. Cahalan, and W. J. Wiscombe: 1994, Bounded cascade models as non-stationary multifractals. *Phys. Rev.*, **E49**, 55–79.
- Marshak, A., A. Davis, W. Wiscombe, and R. Cahalan: 1997, Scale invariance in liquid water distributions in marine stratocumulus. Part ii: multifractal properties and intermittency issues. *J. Atmos. Sci.*, **54**, 1423–1444.
- Martin, G. M., D. W. Johnson, and A. Spice: 1994, The measurement and parameterization of effective radius of droplets in warm stratocumulus clouds. *J. Atmos. Sci.*, **51**, 1823–1842.

- Mason, B. J.: 1952, Production of rain and drizzle in stratiform clouds. *Quart. J. Roy. Meteorol. Soc.*, **78**, 377–386.
- Monin, A. S. and A. M. Yaglom: 1975, *Statistical Fluid Mechanics: Mathematics of Turbulence. Volume 2. (J. L. Lumley ed.)*. MIT Press.
- Nakajima, T., A. Higurashi, K. Kawamoto, and J. E. Penner: 2001, A possible correlation between satellite-derived cloud and aerosol microphysical parameters. *Geophys. Res. Lett.*, **28**, 1171–1174.
- Nicholls, S.: 1984, The dynamics of stratocumulus: aircraft observations and comparisons with a mixed layer model. *Quart. J. Roy. Meteorol. Soc.*, **110**, 783–820.
- 1987, A model of drizzle growth in warm, turbulent, stratiform clouds. *Quart. J. Roy. Meteorol. Soc.*, **113**, 1141–1170.
- Nicholls, S. and J. Leighton: 1986, An observational study of the structure of stratiform cloud sheets: Part i. structure. *Quart. J. Roy. Meteorol. Soc.*, **112**, 431–460.
- Noonkester, V. R.: 1984, Droplet spectra observed in marine stratus cloud layers. *J. Atmos. Sci.*, **41**, 829–845.
- Oreopoulos, L. and R. Davies: 1998, Plane parallel albedo biases from satellite observations. Part i: Dependence on resolution and other factors. *J. Clim.*, **11**, 919–932.
- Paluch, I. R. and D. H. Lenschow: 1991, Stratiform cloud formation in the marine boundary layer. *J. Atmos. Sci.*, **48**, 2141–2158.
- Petty, G. W.: 1995, Frequencies and characteristics of global oceanic precipitation from ship-board present-weather reports. *Bull. Amer. Meteor. Soc.*, **76**, 1593–1616.

- Pincus, R. and S. A. Klein: 2000, Unresolved spatial variability and microphysical process rates in large scale models. *J. Geophys. Res.*, **105**, 27059–27066.
- Pruppacher, H. R. and J. D. Klett: 1997, *Microphysics of clouds and precipitation*. Kuwer Academic Publishers, 976 pp.
- Rand, H. A.: 1995, Mesoscale dynamics of the marine atmospheric boundary layer. *PhD thesis, University of Washington, Seattle, WA, USA*.
- Rogers, D. P., D. W. Johnson, and C. A. Friehe: 1995, The stable internal boundary layer over a coastal sea. Part 1: Airborne measurements of the mean and turbulence structure. *J. Atmos. Sci.*, **52**, 684–696.
- Rotstayn, L. D.: 2000, On the "tuning" of autoconversion parameterizations in climate models. *J. Geophys. Res.*, **105**, 15,495–15,507.
- Schmitt, F., D. Lavallé, D. Schertzer, and S. Lovejoy: 1992, Empirical determination of universal multifractal exponents in turbulent velocity fields. *Phys. Rev. Lett.*, **68**, 305–308.
- Simpson, J. E.: 1997, *Gravity currents in the environment and the laboratory. Second Edition*.
- Snider, J. R., S. Guibert, and J.-L. Brenguier: 2002, Aerosol activation in marine stratocumulus clouds. Part ii: A closure study. *J. Geophys. Res.*, submitted.
- Stephens, G. L., D. G. Vane, R. Boain, G. Mace, K. Sassen, Z. Wang, A. Illingworth, E. O'Connor, W. Rossow, S. L. Durden, S. Miller, R. Austin, A. Benedetti, C. Mitrescu, and the CloudSat Science Team: 2002, The CloudSat mission and the EOS constellation: A new dimension of space-based observations of clouds and precipitation. *Bull. Amer. Meteorol. Soc.*, **83**, 1771–1790.

- Stevens, B., W. R. Cotton, G. Feingold, and C.-H. Moeng: 1998, Large-eddy simulations of strongly precipitating, shallow, stratocumulus-topped boundary layers. *J. Atmos. Sci.*, **55**, 3616–3638.
- Stevens, B., D. Lenschow, G. Vali, H. Gerber, B. Bandy, A. Blomquist, J.-L. Brenguier, C. Bretherton, F. Burnet, T. Campos, S. Chai, I. Faloona, D. Friesen, S. Haimov, K. Laursen, D. Lilly, S. Loehrer, S. Malinowski, B. Morley, M. Petters, D. Rogers, L. Russell, V. Savic-Jovac, J. Snider, D. Straub, M. Szumowski, H. Takagi, D. Thornton, M. Tschudi, C. Twohy, M. Wetzel, and M. van Zanten: 2003, Dynamics and Chemistry of Marine Stratocumulus - DYCOMS II. *Bull. Amer. Meteor. Soc.*, **84**, 579–593.
- Szczodrak, M., P. H. Austin, and P. B. Krummel: 2001, Variability of optical depth and effective radius in marine stratocumulus clouds. *J. Atmos. Sci.*, **58**, 2912–2926.
- Taylor, J. P., G. M. D. J. A. Coakley Jr., W. R. Tahnk, S. Platnick, P. V. Hobbs, and R. J. Ferek: 1999, Effects of aerosols on the radiative properties of clouds. *J. Atmos. Sci.*, **57**, 2656–2670.
- Turton, J. D. and S. Nicholls: 1987, A study of the diurnal variation of stratocumulus using a multiple mixed layer model. *Q. J. R. Meteorol. Soc.*, **113**, 969–1009.
- Twomey, S. and J. Warner: 1967, Comparison of measurements of cloud droplets and cloud nuclei. *J. Atmos. Sci.*, **24**, 702–703.
- Vali, G., R. D. Kelly, J. French, S. Haimov, D. Leon, and A. McIntosh, R. E. Pazmany: 1998, Finescale structure and microphysics of coastal stratus. *J. Atmos. Sci.*, **55**, 3540–3564.
- Van Zanten, M. C., B. Stevens, G. Vali, and D. Lenschow: 2002, The total water budget

- of nocturnal stratocumulus. *Proc. 15th Symposium on Boundary Layers and Turbulence*, Wageningen, The Netherlands.
- 2004, Drizzle paper from dycoms. *J. Atmos. Sci.*.
- Wood, R.: 2000, Parametrization of the effect of drizzle upon the droplet effective radius in stratocumulus clouds. *Quart. J. Roy. Meteorol. Soc.*, **126**, 3309–3324.
- Wood, R. and P. R. Field: 2000, Relationships between total water, condensed water, and cloud fraction in stratiform clouds examined using aircraft data. *J. Atmos. Sci.*, **57**, 1888–1905.
- Wood, R., P. R. Field, and W. R. Cotton: 2002, Autoconversion rate bias in boundary layer cloud parameterizations. *Atmos. Res.*, **65**, 109–128.
- Wood, R. and D. L. Hartmann: 2003, Mesoscale variability of liquid water path in marine boundary layer clouds: Part I. *J. Atmos. Sci.*, in preparation.
- Wood, R. and J. P. Taylor: 2001, Liquid water path variability in unbroken marine stratocumulus. *Quart. J. Roy. Meteorol. Soc.*, **127**, 2635–2662.
- Wyngaard, J. C. and R. A. Brost: 1984, Top-down and bottom-up diffusion of a scalar in the convective boundary layer. *J. Atmos. Sci.*, **41**, 102–112.
- Yum, S. S. and J. G. Hudson: 2002, Maritime/continental microphysical contrasts in stratus. *Tellus*, **B54**, 61–73.
- Yum, S. S., J. G. Hudson, and Y. Xie: 1998, Cloud condensation nuclei and drizzle. *Proc. AMS Conference on Cloud Physics*, Everett, USA, p267–270.

Table 1: Flight numbers, dates, locations, times, cloud type, mean heights of cloud base $\overline{z_{CB}}$ and cloud top ($\overline{z_i}$), mean liquid water path \overline{LWP} (\pm error), mean in-cloud droplet concentration N_* and mean cloud base precipitation rate R_{CB} . Note that the errors are errors in the mean value rather and not estimates of the variability in that parameter.

Flight	Date	Location	Time	Type	$\overline{z_{CB}}$	$\overline{z_i}$	\overline{LWP}	N_*	R_{CB}
			[local]		[m]	[m]	[g m ⁻²]	[cm ⁻³]	[mm d ⁻¹]
A049	6 Dec 90	SW of UK	12-15	Sc	825±23	1450±34	260±44	310	0.49
A209	12 Jun 92	Azores	00-04	Sc	310±44	705±27	170±34	120	0.47
A439	29 Feb 96	NW Ireland	12-15	Sc	780±19	1150±9	100±15	90	0.24
A641	3 Dec 98	North Sea	11-16	Sc	430±7	1110±14	360±16	420	0.054
A644	14 Dec 98	SW of UK	12-15	St	150±75	1800 ¹	90±50	20	0.66
A648	28 Jan 99	SW of UK	12-15	St	190±18	1550 ¹	85±50	8	1.12
A649	29 Jan 99	SW of UK	12-16	Sc	450±9	775±13	80±6	60	0.095
A693	8 Jul 99	NW Ireland	12-16	St/Sc	115±21	395±3	80±3	110	0.41
A762	12 Jun 00	SW of UK	12-16	St/Sc	180±13	495±11	80±5	95	0.28
A763	14 Jun 00	SW of UK	12-16	St/Sc	245±18	485±14	45±2	85	0.34
A764	15 Jun 00	SW of UK	12-16	St/Sc	≈20 ²	320±6	70±6	65	0.44
A767	28 Jun 00	North Sea	12-15	Sc w/Cu	935±24	1350±10	90±10	110	0.78

Notes: 1. The cloud consisted of two or more layers which were heterogeneous and often had indistinct vertical boundaries. The figure for mean cloud top given is for the uppermost layer. 2. The aircraft was not able to descend to cloud base due to visibility restrictions. This cloud base was estimated by extrapolation of the profiles of liquid water content from higher levels.

Table 2: Thermodynamic and dynamic details of the cases studied. From left to right: sea surface temperature SST ; 10 metre wind speed U_{10} ; friction velocity u_* ; mean in-cloud value of the vertical wind speed standard deviation $\overline{\sigma_w}$; mean in-cloud vertical wind integral scale $\overline{\lambda_w}$; ratio of inversion height to the Monin Obukhov length $-z_i/L_{MO}$; mean inversion jump in virtual potential temperature $\Delta\theta_v$; mean inversion jump in total water content Δq_T .

Case	SST [K]	U_{10} [m s ⁻¹]	u_* [m s ⁻¹]	w_* [m s ⁻¹]	$\overline{\sigma_w}$ [m s ⁻¹]	$\overline{\lambda_w}$ [m]	$-z_i/L_{MO}$ [m]	$\Delta\theta_v$ [K]	Δq_T [g kg ⁻¹]
A049	283.3	5.1	0.19	0.63	0.58	175	14.6	5.7	-2.0
A209	290.3	8.1	0.26	0.66	0.70	150	40.9	2.9	-1.0
A439	281.6	6.2	0.25	0.89	0.59	130	18.0	5.5	-3.6
A641	282.5	0.7	0.13	0.97	0.65	230	166	4.3	-0.5
A644	284.7	9.7	0.47	-	0.37	200	-0.50	n/a ¹	n/a ¹
A648	283.9	13.3	0.37	0.33	0.25	200	0.28	n/a ¹	n/a ¹
A649	283.6	2.2	0.14	0.62	0.28	180	34.8	2.7	-1.1
A693	286.4	10.7	0.34	0.43	0.38	35	0.81	5.4	-0.8
A762	286.5	11.3	0.40	-	0.30	60	-0.27	4.4	-0.9
A763	287.2	7.3	0.18	-	0.26	160	-0.84	4.8	-0.3
A764	287.7	1.3	0.14	0.44	0.28	80	12.4	2.3	-0.5
A767	285.1	10.1	0.38	0.95	0.50	130	6.25	3.6	-2.7

¹ These cases contained multiple weak inversions ($\Delta\theta_v < 1$ K; $\Delta q_T < 0.5$ g kg⁻¹) both in and above the cloud layers and it is therefore not possible to define a good measure of the inversion jumps.

Table 3: Values of mean in-cloud total water content q_* , cloud base pressure p_{CB} , temperature T_{CB} and ratio of observed to adiabatic LWP f_{ad} . The error in f_{ad} , given at the 1- σ level, is estimated using a simple model of cloud structure (see text).

Case	q_* [g kg ⁻¹]	p_{CB} [hPa]	T_{CB} [K]	f_{ad}
A049	5.1	928	275.5	0.60 ± 0.10
A209	10.1	987	287.3	0.92 ± 0.18
A439	4.6	940	273.9	0.77 ± 0.08
A641	3.1	960	270.7	0.99 ± 0.04
A644	8.4	996	285.1	0.08 ± 0.09
A648	6.6	993	282.0	0.14 ± 0.08
A649	6.6	972	279.7	0.72 ± 0.05
A693	9.6	1005	286.0	0.77 ± 0.03
A762	9.4	998	286.0	0.67 ± 0.04
A763	9.2	993	285.7	0.67 ± 0.02
A764	8.9	1011	285.0	0.59 ± 0.05
A767	4.8	909	274.6	0.64 ± 0.07

Table 4: In-cloud mean drizzle drop concentration $\overline{N_{d,D}}$, liquid water content $\overline{q_{L,D}}$ and precipitation rate \overline{R} . Also given are cloud top ($0.8 < z_* < 1.0$) and cloud base ($0.0 < z_* < 0.2$) values of the drizzle drop volume radius $r_{v,D}$

Case	$\overline{N_{d,D}}$ [l^{-1}]	$\overline{q_{L,D}}$ [10^{-3} g m^{-3}]	\overline{P} [mm day^{-1}]	$r_{v,D}$ (base) [μm]	$r_{v,D}$ (top) [μm]
A049	37	11.3	0.51	53	38
A209	60	11.2	0.39	46	29
A439	30	7.5	0.26	45	35
A641	18	2.2	0.08	31	29
A644	59	20.9	0.99	42	43
A648	147	30.9	0.80	53	32
A649	46	6.8	0.17	38	30
A693	135	17.6	0.32	37	28
A762	170	17.7	0.28	36	26
A763	118	15.3	0.27	39	27
A764	89	21.8	0.58	44	35
A767	141	21.0	0.67	53	25

Figure captions

Figure 1: Precipitation rate ($R(z_{CB})$, nominally at cloud base) as a function of the cloud droplet concentration N_d in boundary layer clouds. The data are collated using a number of field programs around the world, using mainly *in-situ* aircraft data, but also include recent remote sensing observations. Those measurements for which LWP data are available are shaded with high LWP being darker. The published data are taken from ASTEX Lagrangian 1 (Bretherton and Pincus, 1995), Dycoms II (Van Zanten et al., 2002), North Sea stratocumulus (Nicholls and Leighton, 1986), EPIC (Bretherton et al., 2004), and averages from a number of field campaigns (Yum et al., 1998). Yum and Hudson (2002) measurements were presented as drizzle liquid water content q_D rather than precipitation rate and converted to precipitation rate using the transformation $R = 38q_D^{1.08}$, the best fit relation ($r = 0.90$) derived from the microphysical observations of twelve flights in this study. The correlation coefficient between $\ln N_d$ and $\ln R(z_{CB})$ is $r = -0.57$, significant at the 99% level.

Figure 2: Profiles of (a) temperature; (b) total water content; (c) liquid water content (line) and cloud fraction (circles); (d) droplet concentration for flight A644. In (a), (b) and (c) circles represent run means from 60 km horizontal runs.

Figure 3: (a) Liquid potential temperature and (b) total water content in-cloud profiles for each of the cases. Layer means are subtracted in each case. The same linestyles and symbols are used throughout this article whenever data from multiple flights are plotted on the same axes.

Figure 4: Profiles of (a) droplet concentration N_d , (b) standard deviation of droplet concentration at each level normalised with the mean at each level; (c) values of the subadiabaticity parameter $(q_{ad} - q_L)/q_{ad}(z_i)$ for which zero represents a perfectly adiabatic cloud. The dotted line represents cloud free conditions; (d) the standard deviation of the liquid water content normalised with the mean at that level. Symbols are the same as for Fig. 3.

Figure 5: The mean ratio of liquid water content to adiabatic liquid water content (adiabaticity ratio) as a function of height in cases A763 (filled circles) and A641 (triangles), using the individual profile method (see text). These clearly show that the adiabaticity ratio is roughly constant through the bulk of the cloud ($0.2 < z_* < 0.9$). The error bars show the error in the mean (95% confidence level) derived only from the spread in the data values from different profiles. The estimated errors in q_L/q_{ad} derived from a simple model of the cloud structure are ± 0.09 and ± 0.07 (95% level) for A641 and A763 respectively which do not differ markedly from the errors derived from the spread in data.

Figure 6: Profiles of mean cloud fraction for all cases. Symbols are as Fig. 3.

Figure 7: Profiles of vertical wind standard deviation for all cases. Symbols are as Fig. 3.

Figure 8: Profiles of characteristics relating to the drizzle drops, which are defined here as drops with radii larger than $20 \mu\text{m}$. (a) Drizzle droplet concentration $N_{d,D}$ normalised with the mean drizzle droplet concentration in the cloud layer; (b) volume radius of drizzle drops $r_{v,D}$

which increases towards cloud base; (c) liquid water content contained in the drizzle drops normalised with the mean value for the cloud layer; (d) precipitation rate normalised with the mean value in the cloud layer. Symbols are as Fig. 3.

Figure 9: Profiles of the vertical turbulent fluxes of total water content (filled circles) and precipitation rates for the 12 cases. Error bars on the turbulent fluxes are estimated using the integral scale method of Lenschow and Stankov (1986). Here $\overline{wq_T}$ is shown positive, and R negative, for upward transport of moisture.

Figure 10: Sub-cloud precipitation rates normalised with cloud base values plotted as a function of height below cloud base normalised with the $r > 20\mu\text{m}$ mean volume radius of the size distribution at cloud base taken from Table 4. The dashed line is a parameterization derived from the sedimentation-evaporation model and constitutes a reasonable fit to the observations.

Figure 11: Sedimentation-evaporation model cooling rates for the evaporation of drizzle below cloud base as a function of height below cloud base and mean volume radius of the drizzle drops at cloud base. The cooling rates are expressed in K day^{-1} per mm day^{-1} of cloud base precipitation rate. A dry adiabatic layer is assumed below cloud base. The dashed line shows the level of the peak cooling rate.

Figure 12: Difference between the mean subcloud virtual potential temperature (θ_v , abscissa) and mean total water (q_T , ordinate) in drizzle regions and drizzle-free regions for suit-

able subcloud runs. The dashed line corresponds to differences caused purely by evaporation.

Figure 13: Cumulative distribution of drizzle cell sizes from all flights for in-cloud and below cloud runs. The ordinate shows the fraction of regions with sizes larger than shown on the abscissa.

Figure 14: Composite normalised power spectrum of precipitation rate from all in-cloud and sub-cloud runs. The dotted lines show the 25th and 75th percentiles. The dashed line shows the best fit power law. Each contributing spectrum was first normalised with its variance and windowed using a Hanning window before compositing.

Figure 15: Mean multifractal plane (lower) and example synthetic spatial series of LWP and drizzle precipitation rate (upper panels). Drizzle is more intermittent (larger C_1 and more stationary (lower H_1) than cloud water fields. The example series were generated using the bounded cascade model described in Marshak et al. (1994) which has properties of both additive and multiplicative cascades.

Figure 16: (a) Relative degree of spatial variability in cloud LWP and precipitation rate denoted by the standard deviation normalized with the mean; (b) Relative degree of spatial variability in cloud droplet concentration.

Figure 17: Stationarity and intermittency parameters H_1 and C_1 for simulated fields $y = LWP^\eta$ as described in the text. Shaded regions show one standard deviation from 100 re-

alisations either side of the mean. The intermittency C_1 increases while H_1 decreases, as η increases. For $3.5 < \eta < 4.5$ the simulated field display stationarity and intermittency characteristic of precipitation fields in drizzling stratocumulus.

Figure 18: Mean adiabaticity f_{ad} of the clouds studied as a function of the ratio of the rainout timescale to the eddy turnover timescale τ_{driz}/τ_w . The error bars show the estimated uncertainties in the two parameters. Also shown are the results from an equilibrium model of drizzle production plotted as a function of τ_{driz}/τ_{rep} where τ_{rep} is the replenishment timescale for cloud LWP (see text).

Figure 19: Scaling of observed drizzle rates with different variables. Dashed lines are relationships derived from two recent field campaigns: (a) DYCOMS-II (Stevens et al., 2003);(b) EPIC 2001 (Bretherton et al., 2004). The cloud thickness is h ; other variables are as defined in this study.

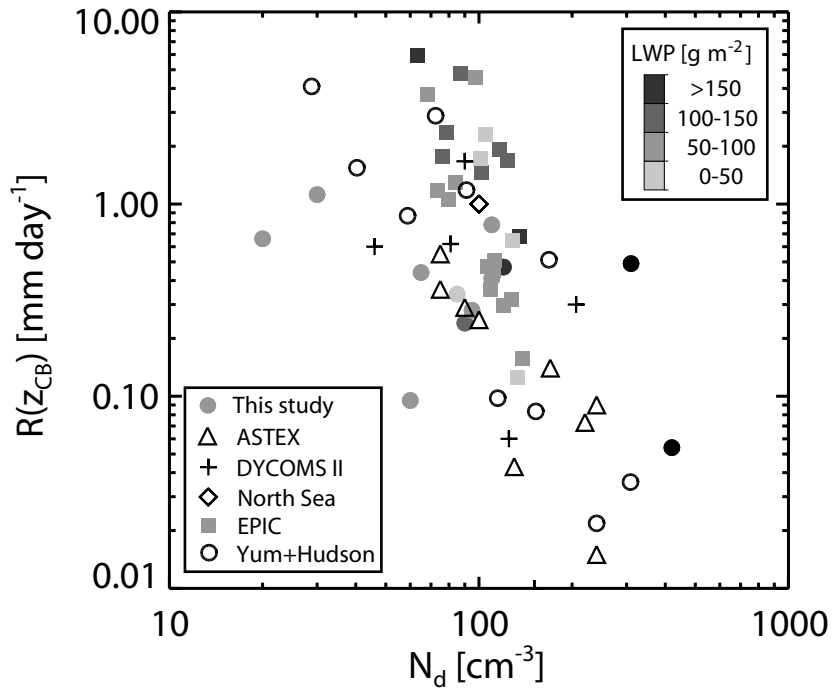


Figure 1:

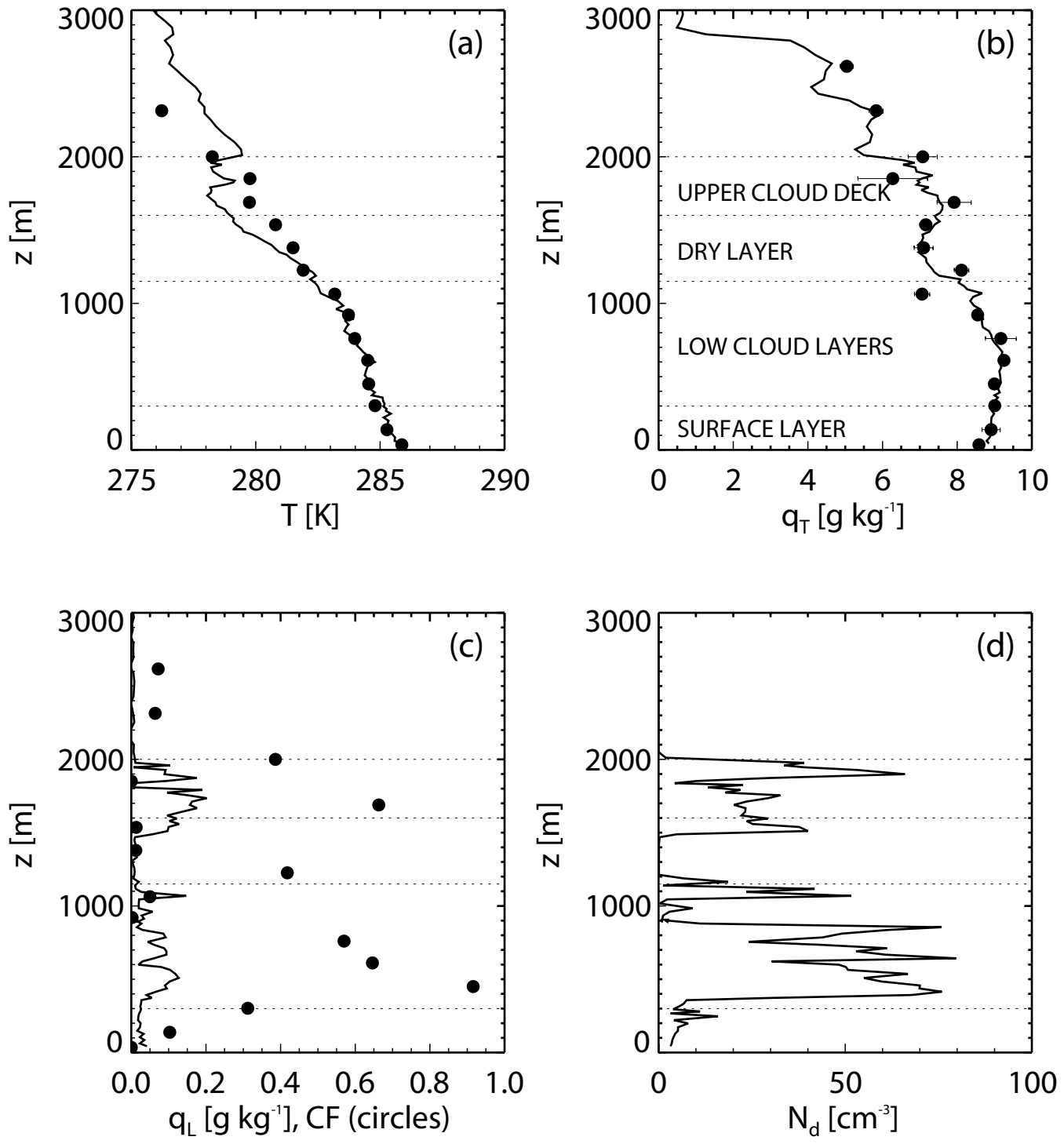
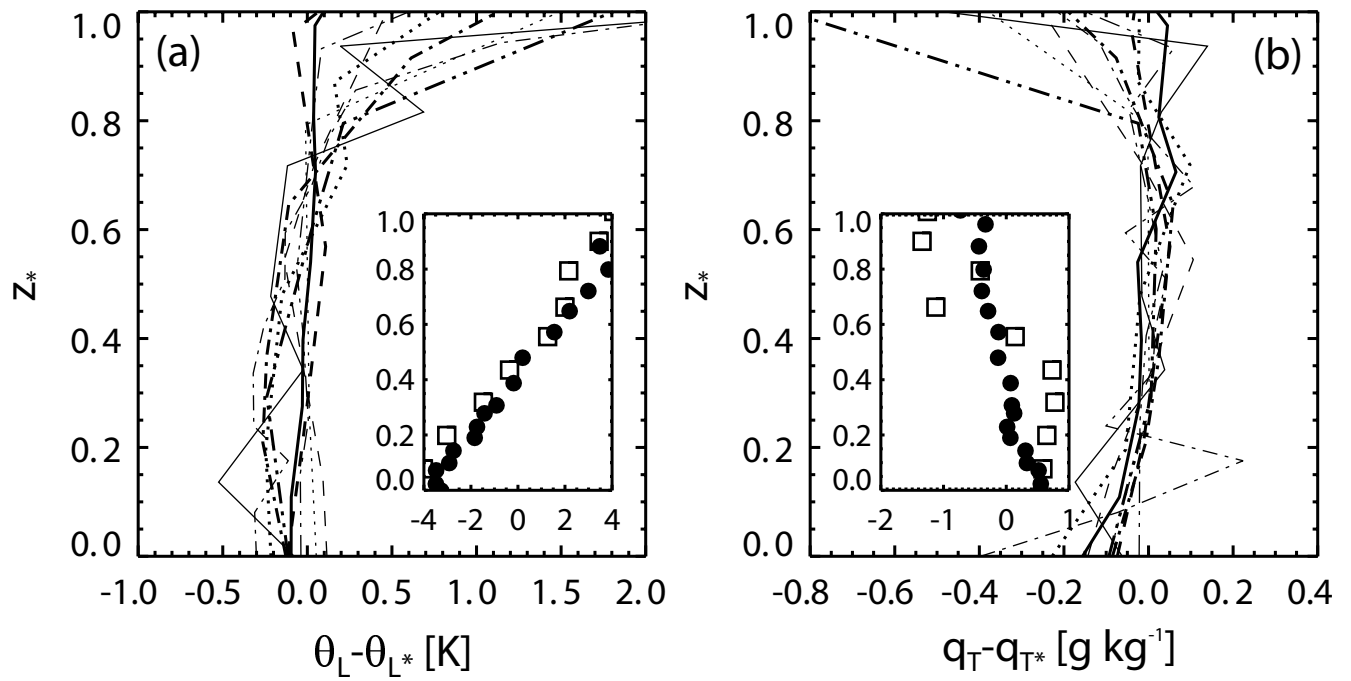


Figure 2:



A049	—————	A644	□	A762
A209	A648	●	A763	----
A439	----	A649	----	A764	----
A641	----	A693	—————	A767	----

Figure 3:

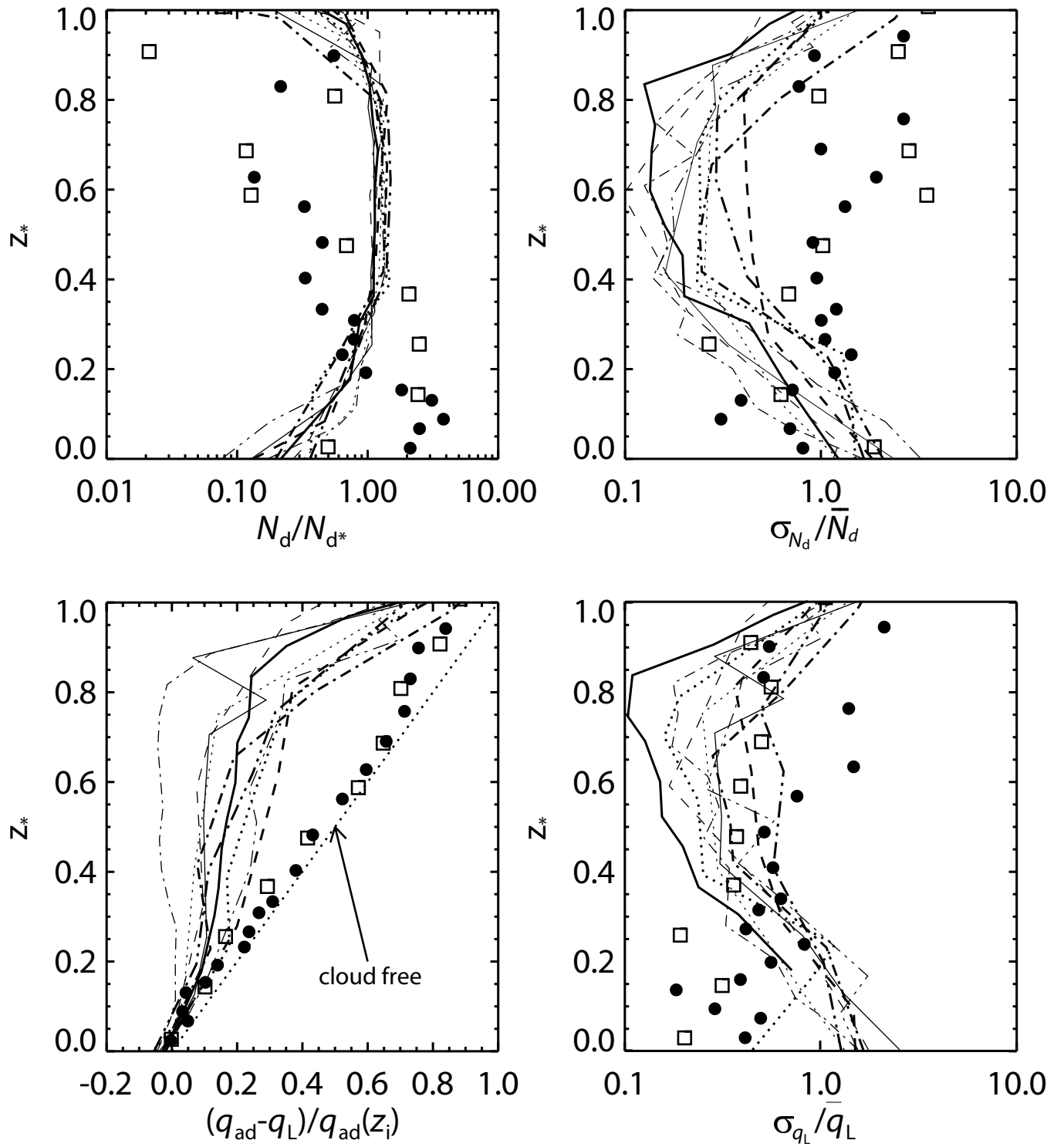


Figure 4:

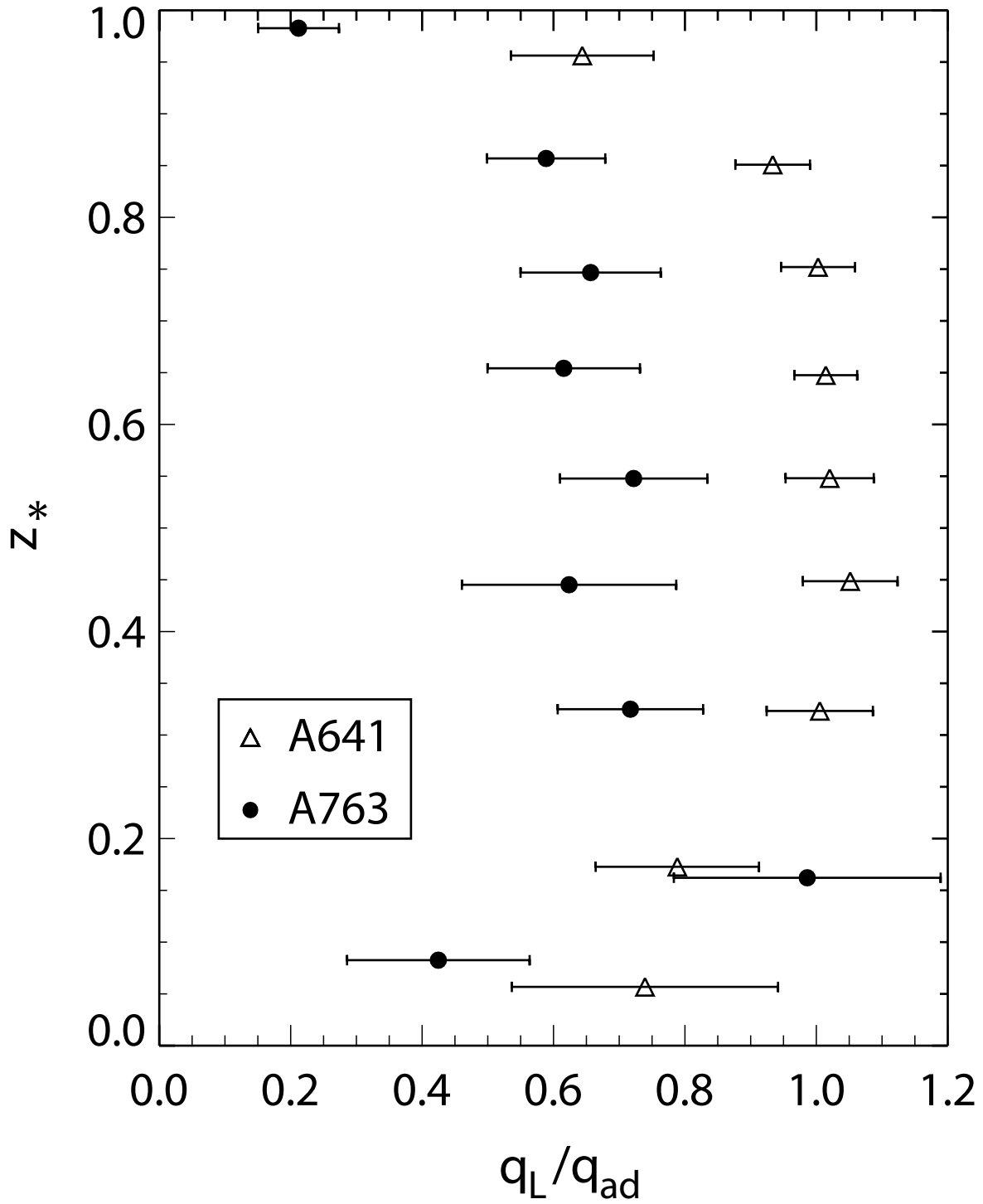


Figure 5:

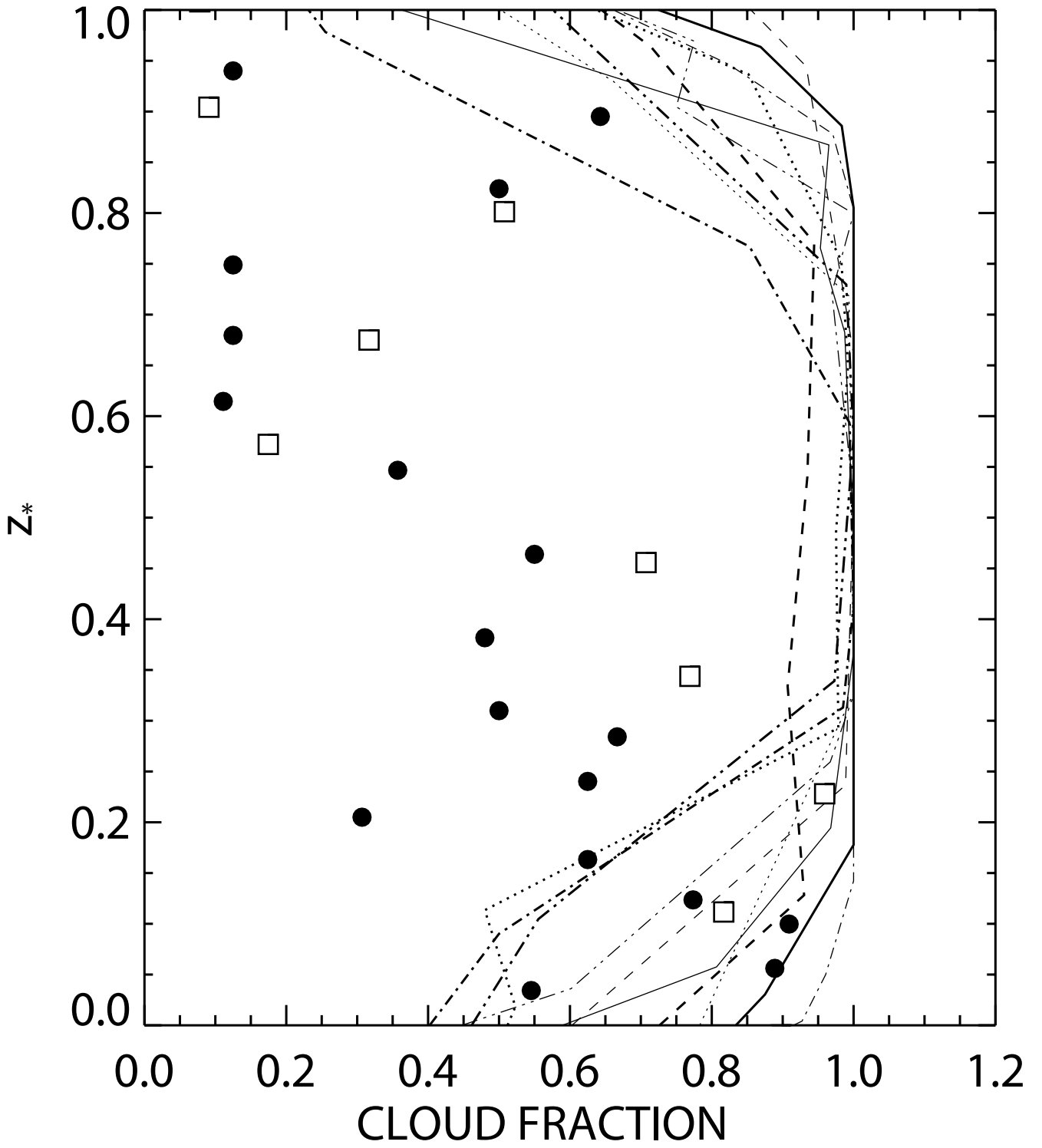


Figure 6:

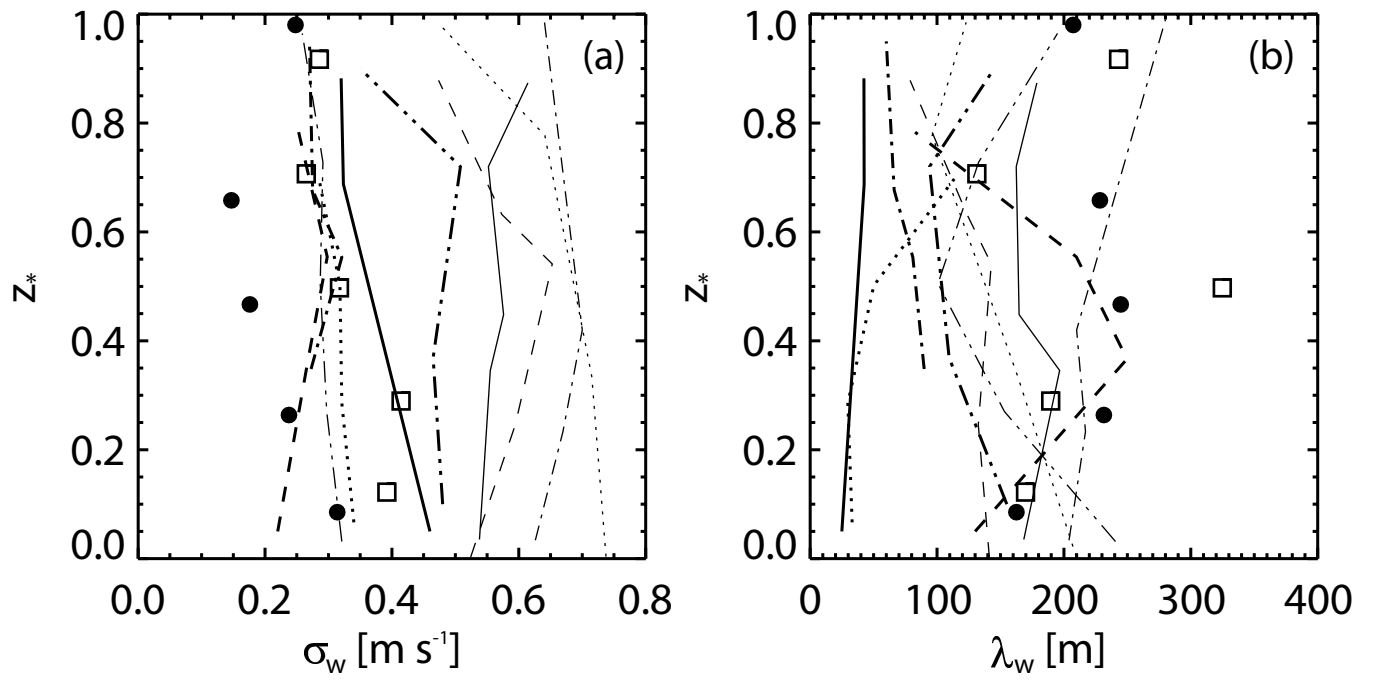


Figure 7:

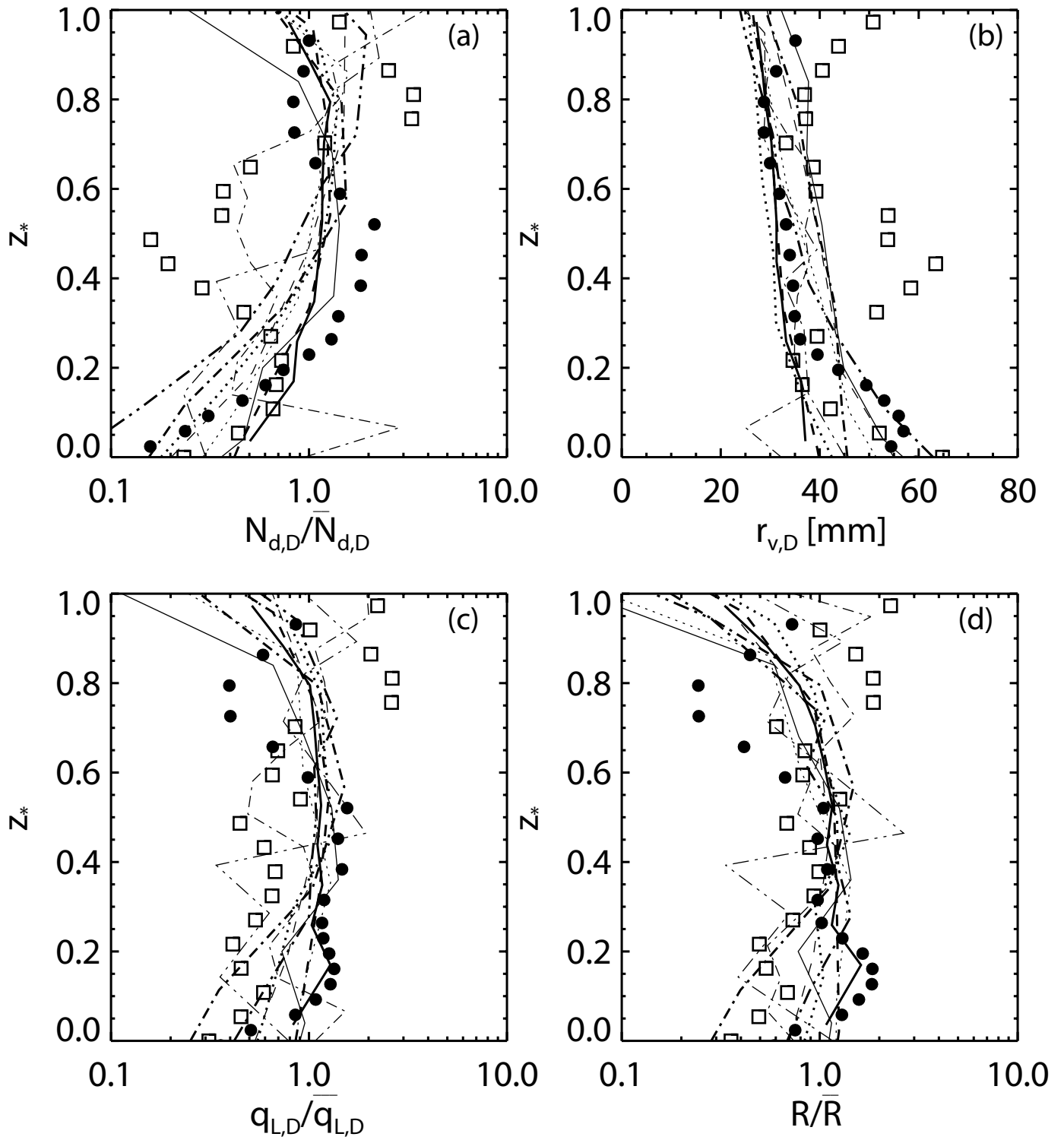


Figure 8:

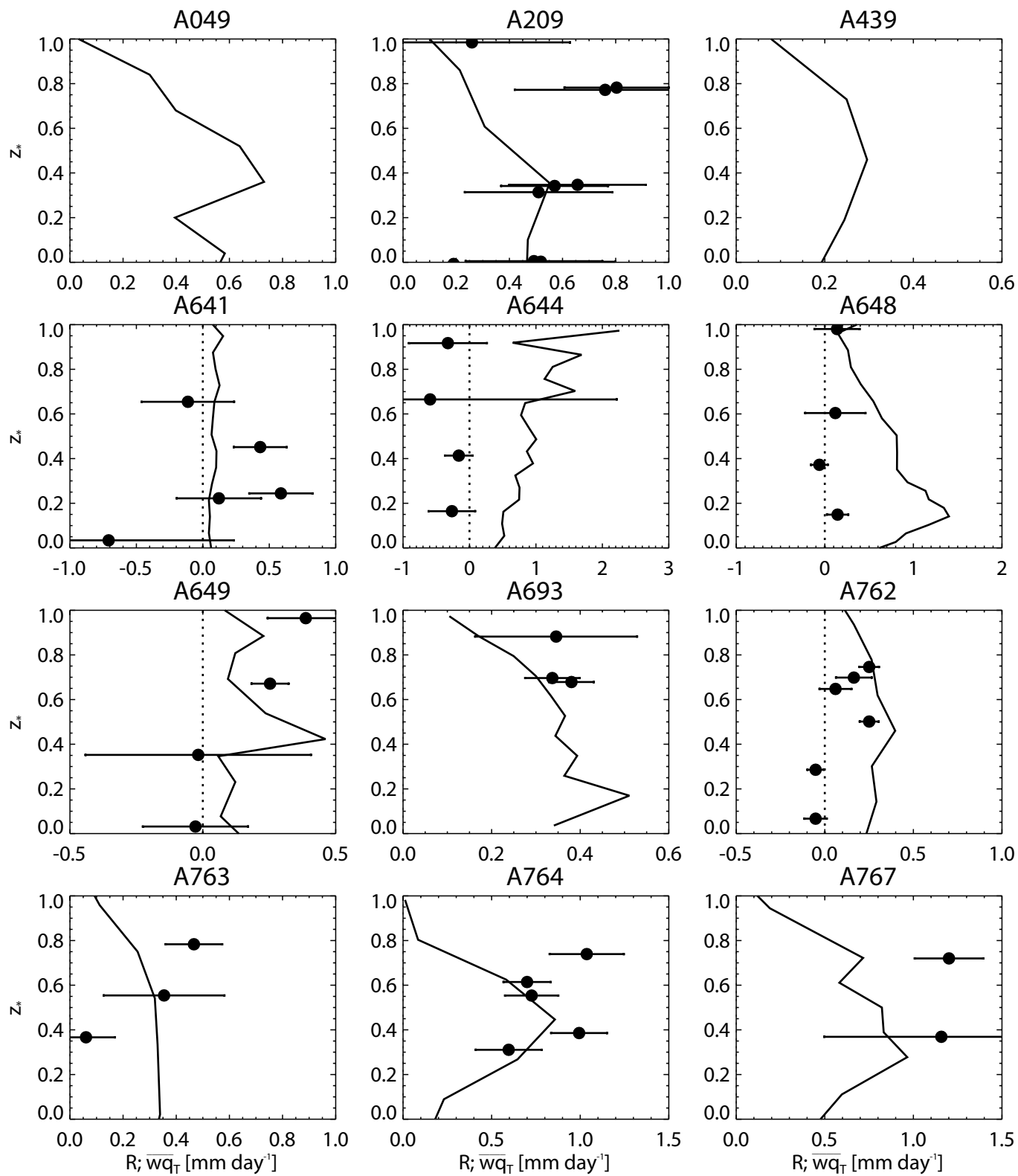


Figure 9:

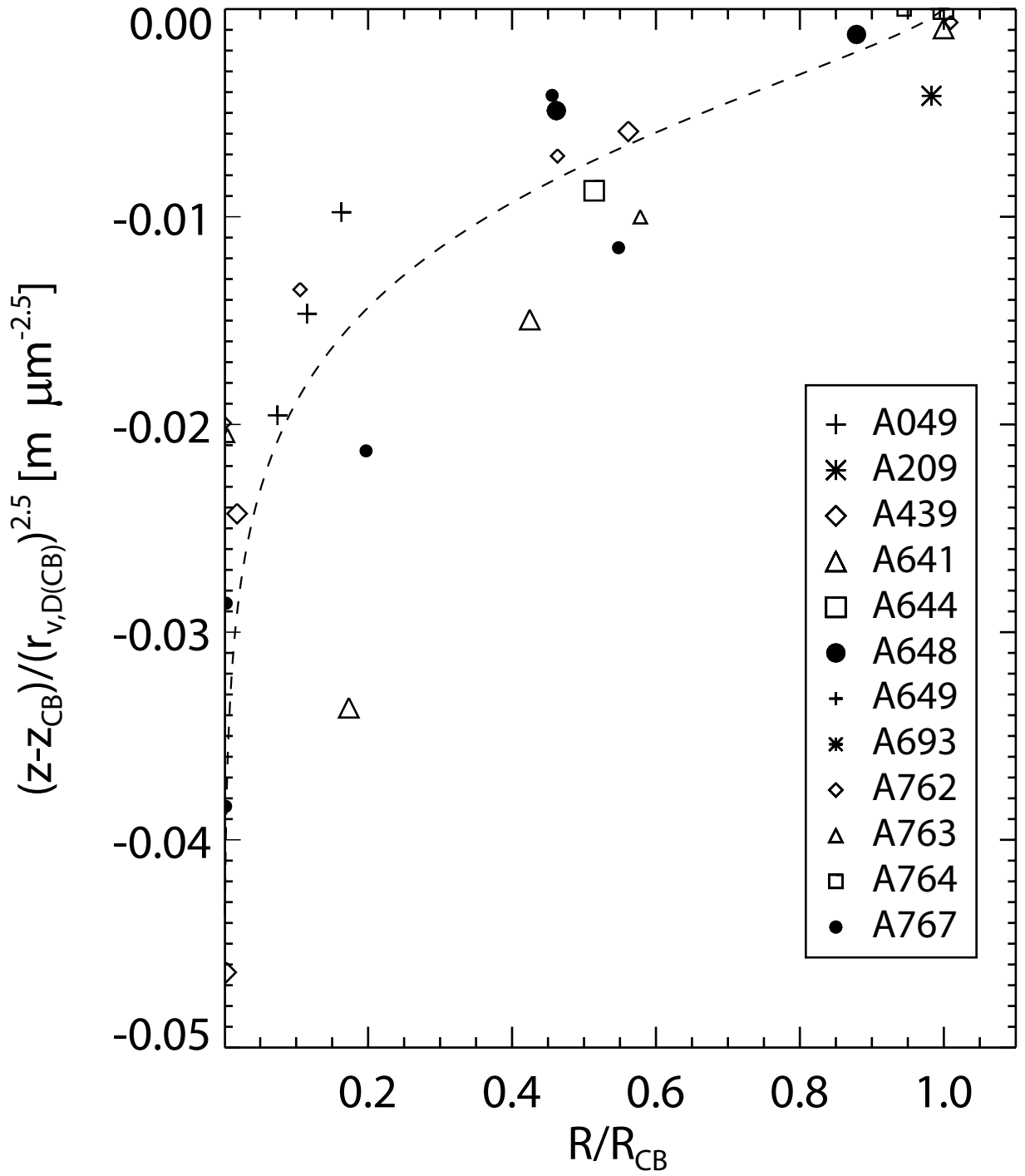


Figure 10:

Evaporative cooling rate [K day^{-1}]
per mm/day R_{CB}

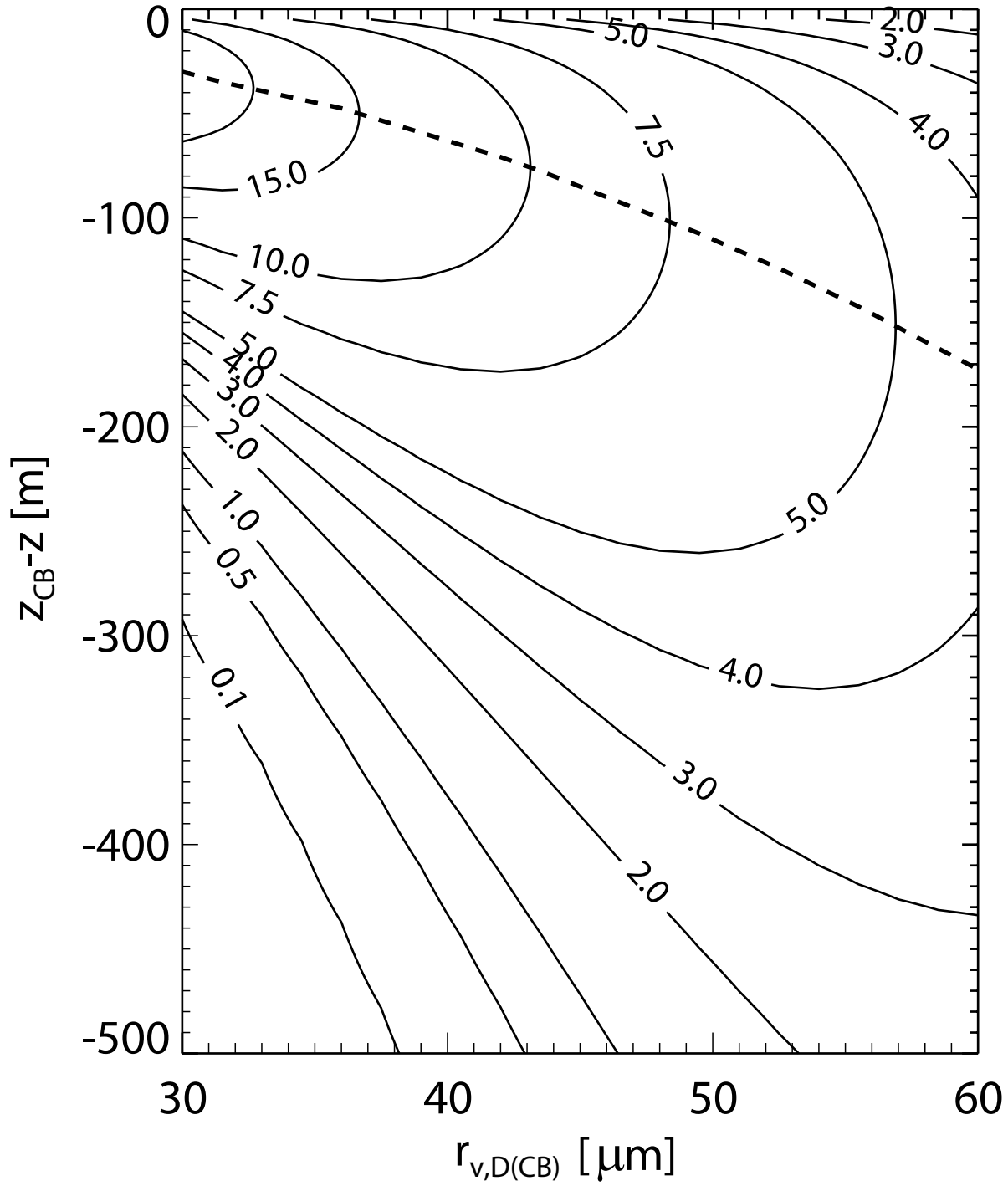


Figure 11:

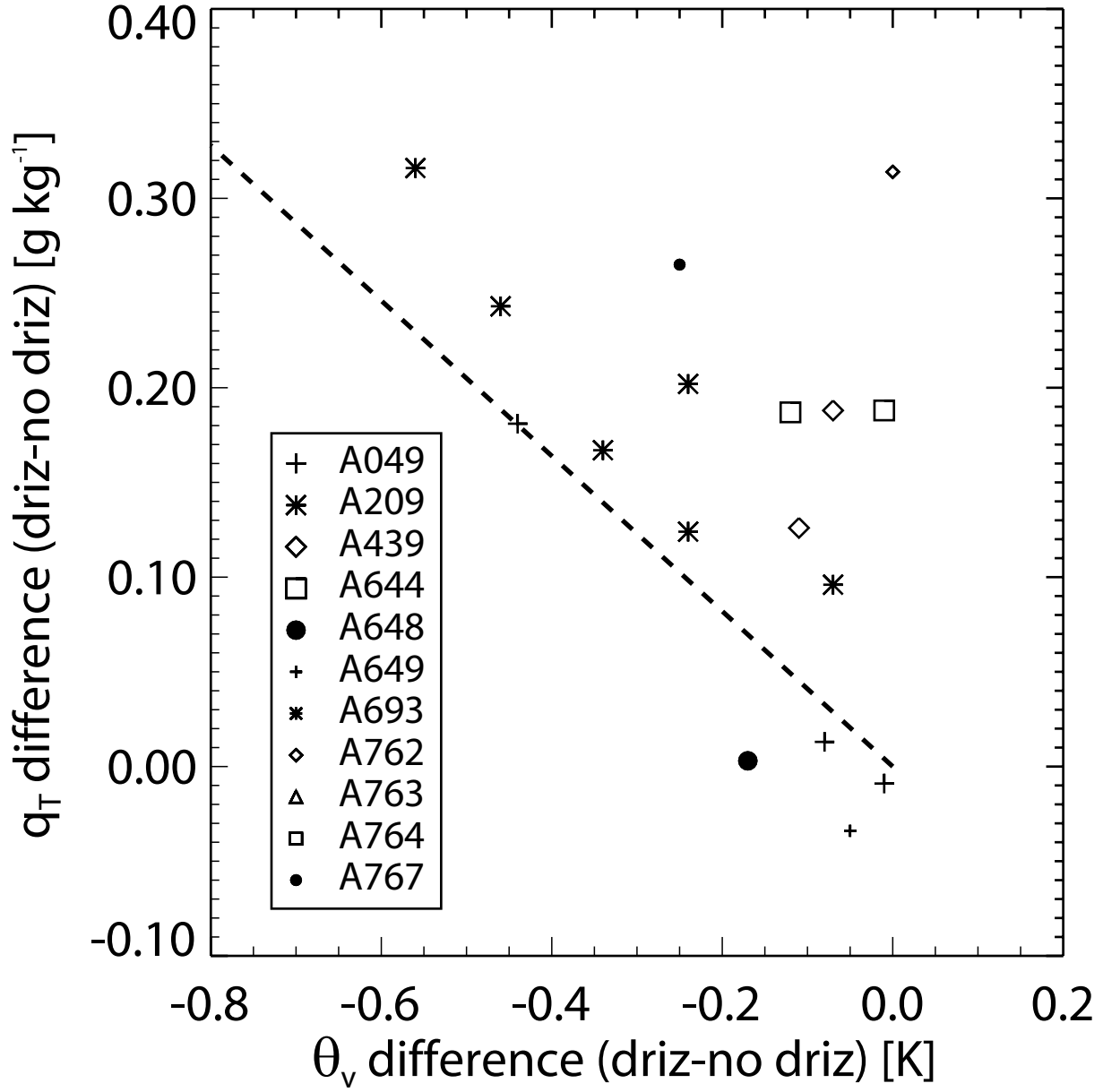


Figure 12:

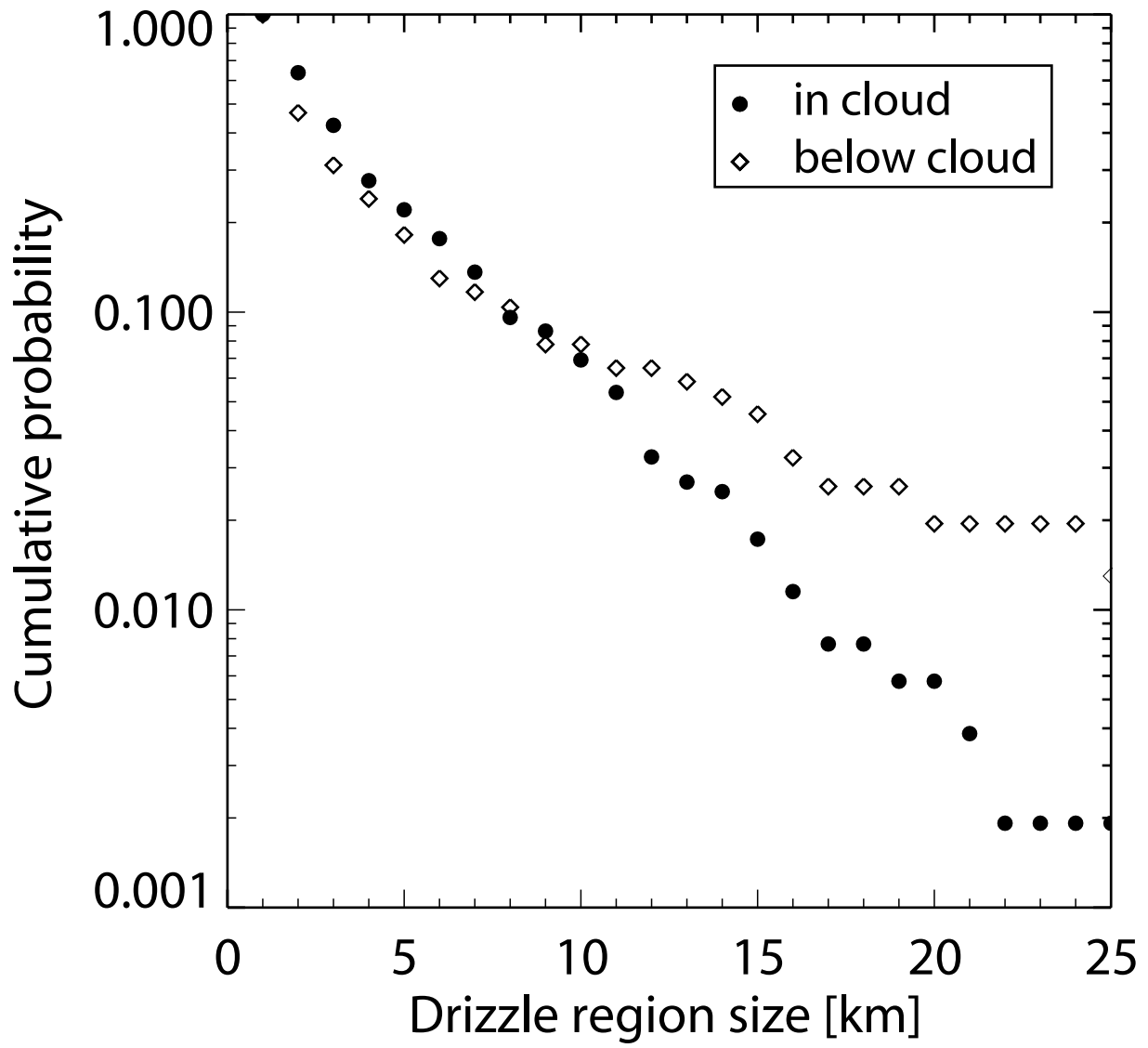


Figure 13:

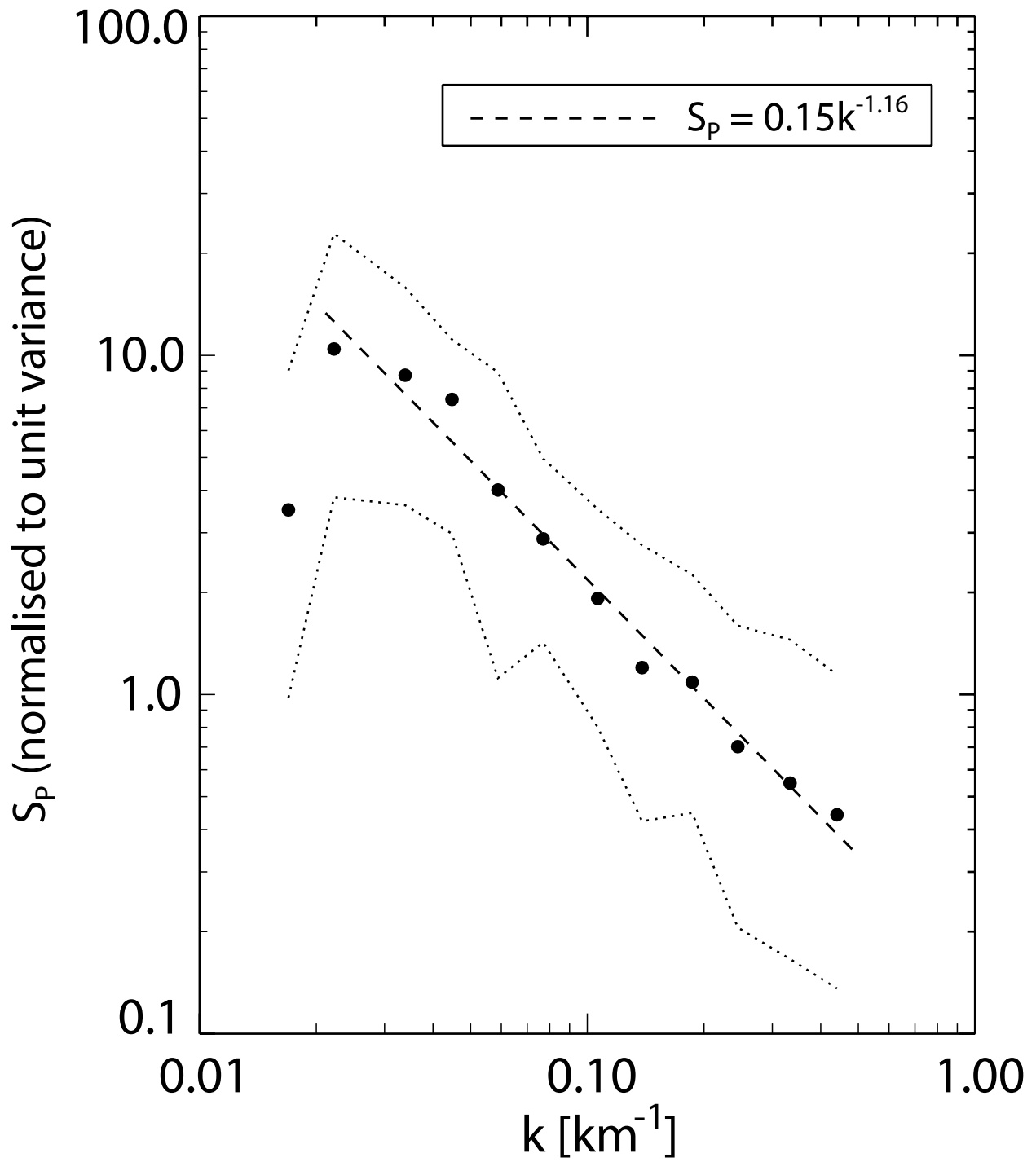


Figure 14:

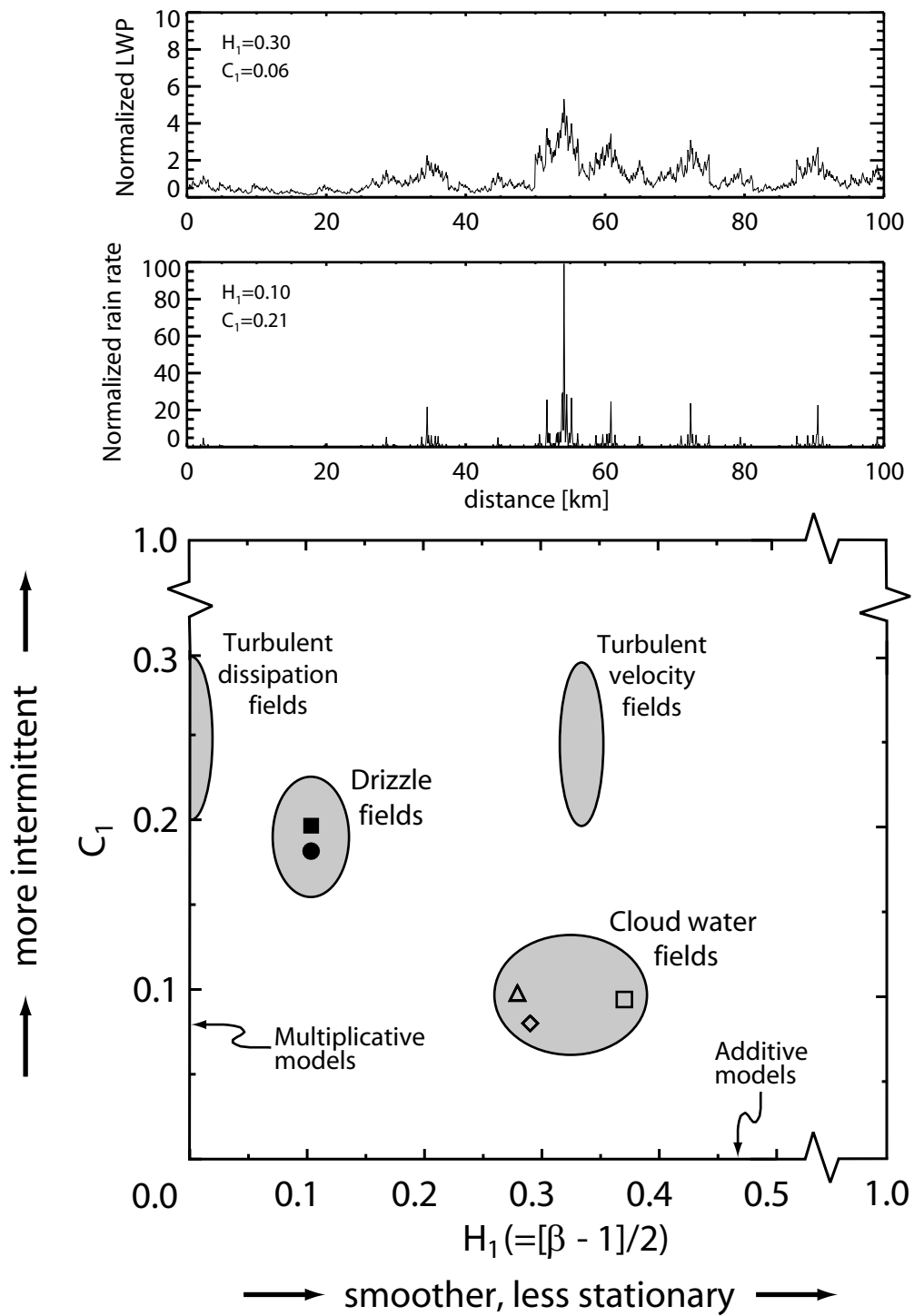


Figure 15:

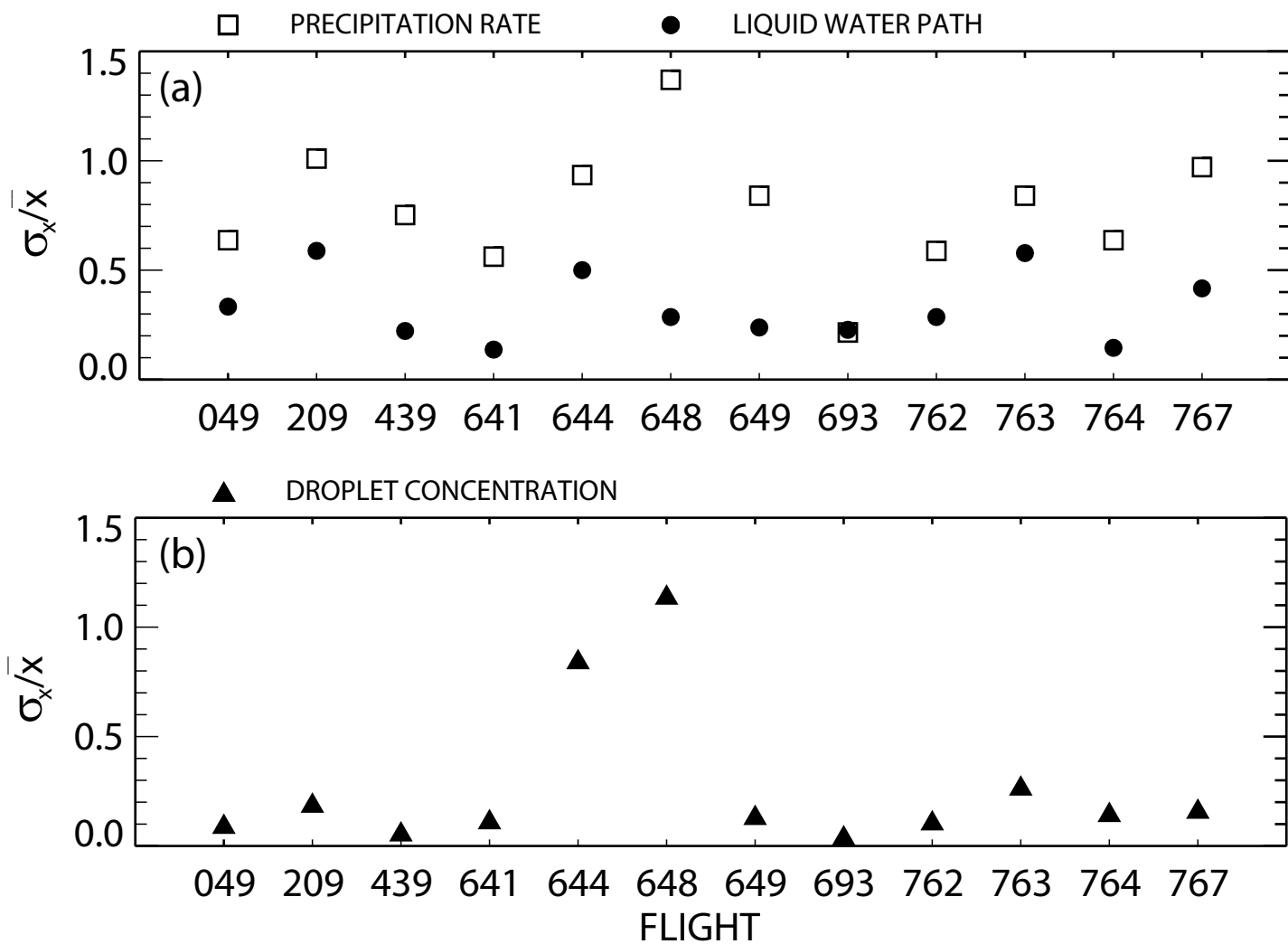


Figure 16:

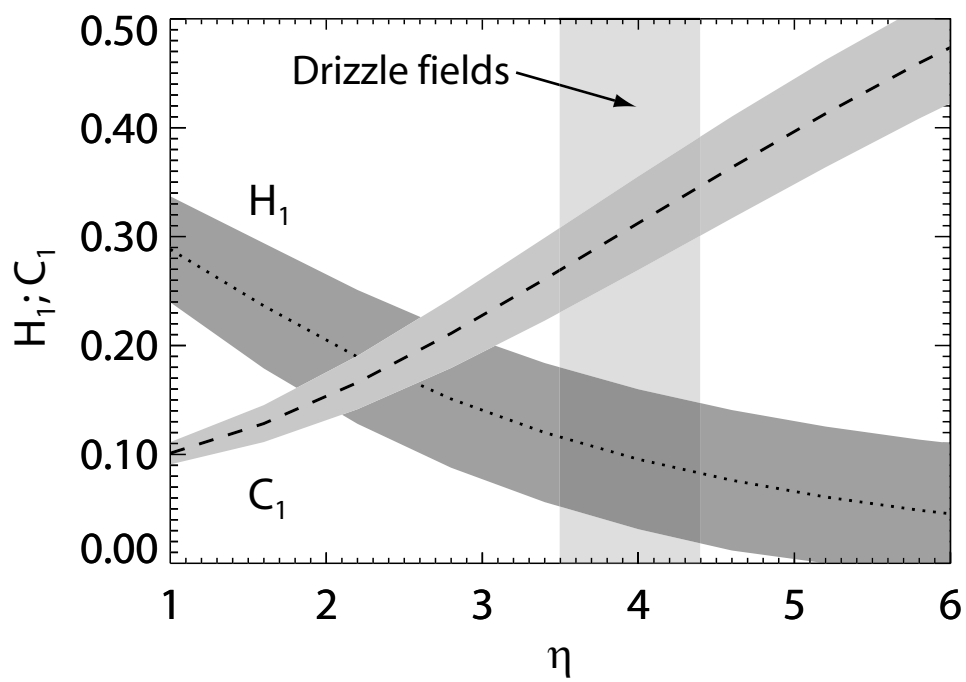


Figure 17:

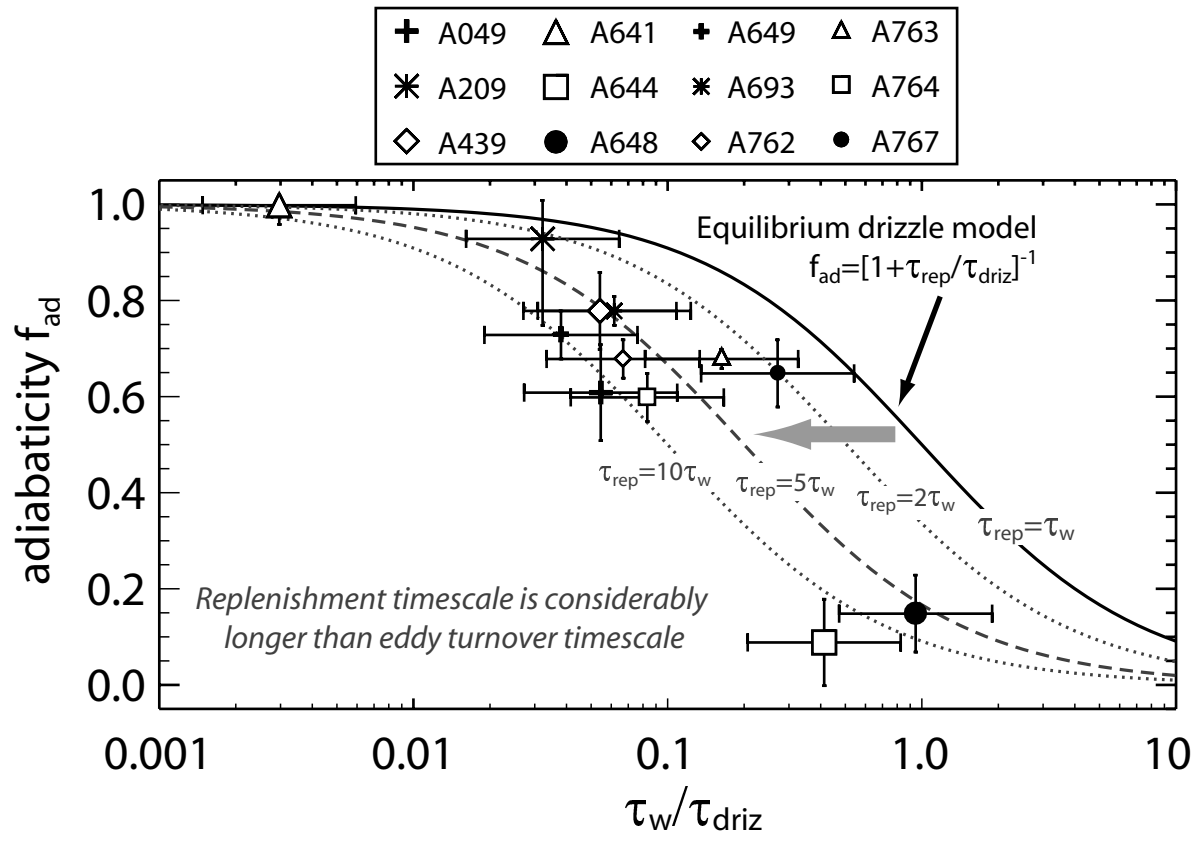


Figure 18:

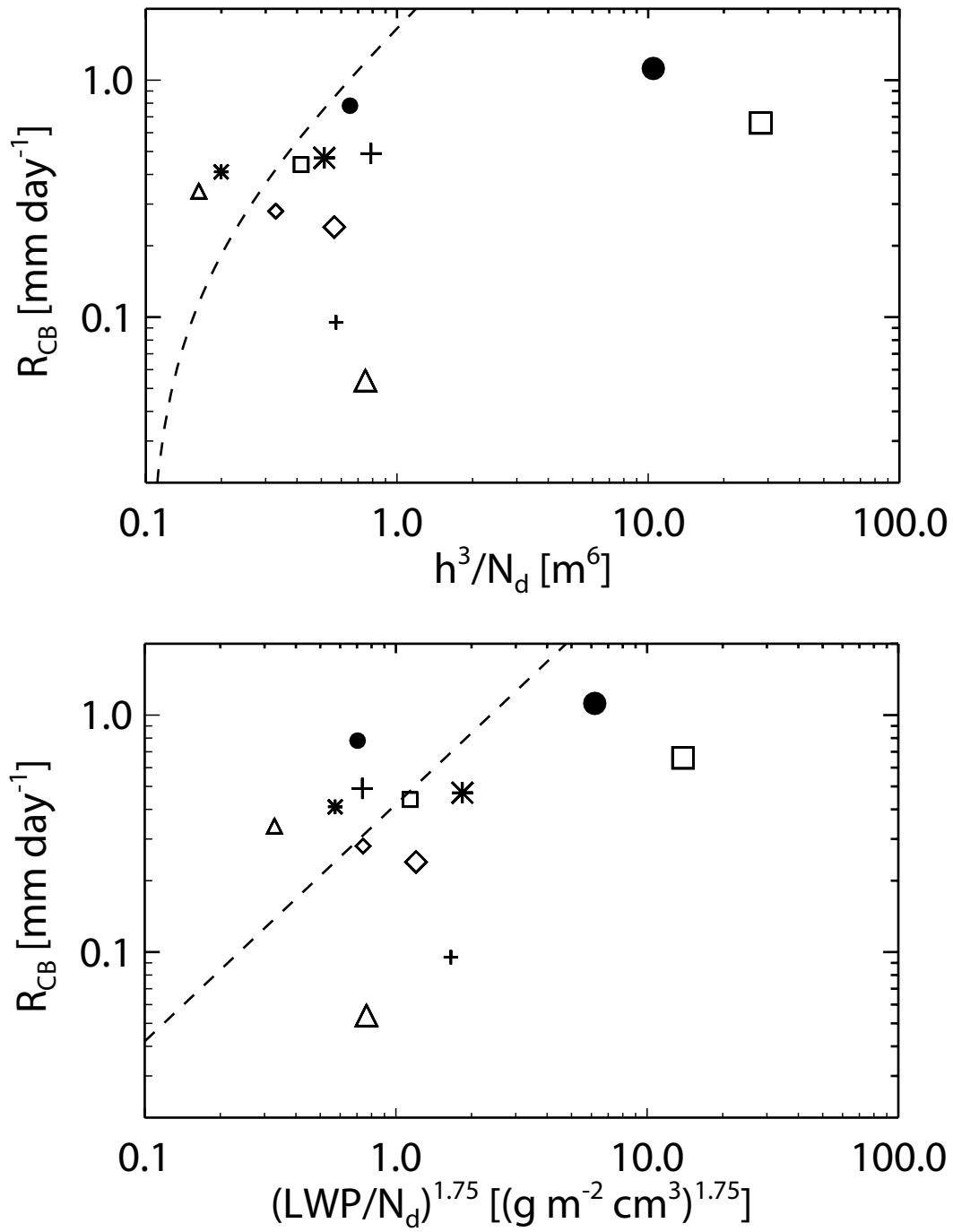


Figure 19: